State-of-the-Art Rotor Aerodynamics and Shipboard Rotorcraft Flight Simulation

Final Report for Sub-contract under
ONR Contract No. N00014-09-C-0814

Sub-contract Report submitted
to
Chengjian He and Jinggen Zhao
Advanced Rotorcraft Technology, Inc.
635 Vaqueros Avenue
Sunnyvale, CA 94085
he@flightlab.com

by
J.V.R. Prasad and L.N. Sankar
Georgia Institute of Technology
j.v.r.prasad@aerospace.gatech.edu

September 15, 2012

1. STABILIZATION OF REDUCED ORDER MODELS

1.1 Development of standard reduced order model based on proper orthogonal decomposition

During this reporting period, efforts were concentrated on the stabilization of a Reduced Order Model (ROM) for the unsteady ship airwake using the combined POD method and a Galerkin projection technique. Starting from an existing unsteady flow-field solution/approximation for the non-dimensional incompressible Navier-Stokes equation

$$\nabla \cdot u = 0 \tag{1}$$

$$\frac{\partial u}{\partial t} = -u \cdot \nabla u - p + \frac{1}{Re}\Delta u \tag{2}$$

The characteristics of the flow-field at any instant of time can be formed as a linear combination of the POD modes (using a total of N_{POD} modes) and the time-averaged mean value as follows:

$$u(t,x,y,z) = u_m + \sum_{i=1}^{N_{POD}} a_i(t)\Phi_i(x,y,z) \tag{3}$$

where $u_m = \sum_{i=1}^{N_s} u_i$ is the time-averaged mean flow-field of all Ns "snapshots" and a_i is the coefficient for the i−*th* POD mode. Substituting Eq. 3 into the governing Navier-Stokes equation (Eq. 2) and using the Galerkin projection

$$< u_t + u \cdot \nabla u, \Phi_i > + < \nabla p - \frac{1}{Re}\nabla \cdot (\nabla u), \Phi_i >= 0$$

For the $< \nabla \cdot (\nabla u), \Phi_i >$ term

$$< (\nabla \cdot (\nabla u)), \Phi_i >= \int (\nabla \cdot (\nabla u)) \cdot \Phi_i \, d\Omega = \int \nabla \cdot (\nabla u \cdot \Phi_i)\, d\Omega - \int \nabla u \cdot \nabla \Phi_i \, d\Omega$$

For pressure term

$$< \nabla p, \Phi_i >= \int \nabla p \cdot \Phi_i \, d\Omega$$

From divergence theorem $\int_\Omega \nabla \cdot \underset{A}{\rightarrow} d\Omega = \int_\Gamma \underset{A}{\rightarrow} \cdot \underset{n}{\rightarrow} d\Gamma$

$$\int \nabla \cdot (\nabla u \cdot \Phi_i)\, d\Omega = \int \left(\nabla u \cdot \underset{n}{\rightarrow} \cdot \Phi_i\right) d\Gamma$$

$$\int \nabla p \cdot \Phi_i \, d\Omega = \int p \cdot \underset{n}{\rightarrow} \cdot \Phi_i \, d\Gamma$$

$$< u_t + u \cdot \nabla u, \Phi_i > + \frac{1}{Re}\int \nabla u \cdot \nabla \Phi_i \, d\Omega + \int p \cdot \underset{n}{\rightarrow} \cdot \Phi_i \, d\Gamma - \frac{1}{Re}\int \left(\nabla u \cdot \underset{n}{\rightarrow} \cdot \Phi_i\right) d\Gamma = 0$$

Finally,

$$< u_t + u \cdot \nabla u, \Phi_i > + \frac{1}{Re} < \nabla u, \nabla \Phi_i > + < p \cdot \underset{n}{\rightarrow} - \frac{1}{Re}\nabla u \cdot \underset{n}{\rightarrow}, \Phi_i > |_{d\Gamma} = 0 \tag{4}$$

In the current study, the integration on the domain boundary is ignored. Therefore, using the orthogonal property of the POD modes ($< \Phi_i, \Phi_j > = \delta_{ij}$) converts the original full Navier-Stokes equation into a ROM which only involves N_{POD} ordinary differential equations (ODEs) as follows:

$$< \frac{\partial u_m}{\partial t} + \frac{\partial a\Phi_j}{\partial t} , \Phi_i > + < \left(u_m + a\Phi_j\right) \cdot \nabla\left(u_m + a\Phi_j\right) , \Phi_i > + \frac{1}{Re} < \nabla\left(u_m + a\Phi_j\right), \nabla\Phi_i >= 0$$

$$\frac{\partial a}{\partial t} + < u_m \cdot \nabla u_m , \Phi_i > + < u_m \cdot \nabla a\Phi_j , \Phi_i > + < a\Phi_j \cdot \nabla u_m , \Phi_i > + < a\Phi_j \cdot \nabla a\Phi_k, \Phi_i > + \frac{1}{Re} < \nabla u_m, \nabla\Phi_i > + \frac{1}{Re} < \nabla a\Phi_j, \nabla\Phi_i >= 0 \quad (5)$$

By rearrange Eq. 5,

$$\frac{\partial a}{\partial t} = Aa + a^T Qa + E \quad (6)$$

$$a(0) = a_0 \quad (7)$$

$$A = - < \Phi_j \cdot \nabla u_m , \Phi_i > - < u_m \cdot \nabla\Phi_j , \Phi_i > - \frac{1}{Re} < \nabla\Phi_j, \nabla\Phi_i > \quad (8)$$

$$Q = - < \Phi_j \cdot \nabla\Phi_k, \Phi_i > \quad (9)$$

$$E = - < u_m \cdot \nabla u_m , \Phi_i > - \frac{1}{Re} < \nabla u_m, \nabla\Phi_i > \quad (10)$$

where $a = [a_1, a_2, \cdots a_{NPOD}]^T$ is the collection of all N_{POD} POD mode coefficients; A and Q are the linear and quadratic term matrices, respectively; E is the constant term; and a_0 are the initial values.

1.2 A pressure extended reduced order model

As pointed out in Ref. [1], the effect of the pressure term may be important for convectively unstable shear flows such as the wake flow. Therefore, a pressure-extended ROM model similar to that proposed in Ref. [2] was implemented and investigated. The theory of the pressure extended ROM is first discussed in this section. Similarly to unsteady velocities, the unsteady pressure term can be also decomposed using the POD techniques as follows:

$$p(t, x, y, z) = p_m + \sum_{i=1}^{N_{POD}} a_i(t)\Psi_i(x, y, z) \quad (11)$$

Substituting the POD representations for both the velocity and the pressure (Eqs.3 and 11) into the governing Navier-Stokes equation (Eq. 2) gives rise to

$$\frac{\partial(u_m + a_j\Phi_j)}{\partial t} = -\left(u_m + a_j\Phi_j\right) \cdot \nabla\left(u_m + a_j\Phi_j\right) - \nabla\left(p_m + a_j\Psi_j\right) + \frac{1}{Re}\Delta\left(u_m + a_j\Phi_j\right)$$

$$\Phi_j \frac{\partial a_i}{\partial t} = - u_m \cdot \nabla u_m - a_j u_m \cdot \nabla\Phi_j - a_j\Phi_j \cdot \nabla u_m - a_j\Phi_j \cdot \nabla\Phi_j a_j - \nabla p_m - a_j\nabla\Psi_j + \frac{1}{Re}\Delta u_m + a_j \frac{1}{Re}\Delta\Phi_j \quad (12)$$

Galerkin projection of Eq. 12 give rise to

$$\langle\Phi_j, \Phi_i\rangle \frac{\partial a_j}{\partial t} = -\langle u_m \cdot \nabla u_m, \Phi_i\rangle - \langle\nabla p_m, \Phi_i\rangle + \frac{1}{Re}\langle\Delta u_m, \Phi_i\rangle$$

$$-a_j\left\{\langle u_m \cdot \nabla\Phi_j, \Phi_i\rangle + \langle\Phi_j \cdot \nabla u_m, \Phi_i\rangle + \langle\nabla\Psi_j, \Phi_i\rangle - \frac{1}{Re}\langle\Delta\Phi_j, \Phi_i\rangle\right\} - a_j\langle\Phi_j \cdot \nabla\Phi_k, \Phi_i\rangle a_i \quad (13)$$

By using Divergence theorem

$$\langle\frac{1}{\mathrm{Re}}\Delta\left(\mathrm{u_m}+\mathrm{a_j}\Phi_\mathrm{j}\right),\Phi_\mathrm{i}\rangle=\langle\frac{1}{\mathrm{Re}}\nabla\cdot\left(\nabla\mathrm{u_m}+\mathrm{a_j}\nabla\Phi_\mathrm{j}\right),\Phi_\mathrm{i}\rangle=\frac{1}{\mathrm{Re}}\langle\nabla\cdot\nabla\mathrm{u_m},\Phi_\mathrm{i}\rangle+\mathrm{a_j}\frac{1}{\mathrm{Re}}\langle\nabla\cdot\nabla\Phi_\mathrm{j},\Phi_\mathrm{i}\rangle$$

For $<\nabla\cdot(\nabla\mathrm{u}),\Phi_\mathrm{i}>$ term

$$<(\nabla\cdot(\nabla\mathrm{u})),\Phi_\mathrm{i}>=\int(\nabla\cdot(\nabla\mathrm{u}))\cdot\Phi_\mathrm{i}\ \mathrm{d}\Omega=\int\nabla\cdot(\nabla\mathrm{u}\cdot\Phi_\mathrm{i})\,\mathrm{d}\Omega-\int\nabla\mathrm{u}\cdot\nabla\Phi_\mathrm{i}\,\mathrm{d}\Omega$$

$$\langle\frac{1}{\mathrm{Re}}\nabla\cdot\left(\nabla\mathrm{u_m}+\mathrm{a_j}\nabla\Phi_\mathrm{j}\right),\Phi_\mathrm{i}\rangle=\frac{1}{\mathrm{Re}}\langle\nabla\cdot\nabla\mathrm{u_m},\Phi_\mathrm{i}\rangle-\frac{1}{\mathrm{Re}}\langle\nabla\mathrm{u_m},\nabla\Phi_\mathrm{i}\rangle+\mathrm{a_i}\frac{1}{\mathrm{Re}}\langle\nabla\cdot\nabla\Phi_\mathrm{j},\Phi_\mathrm{i}\rangle-\mathrm{a_j}\frac{1}{\mathrm{Re}}\langle\nabla\Phi_\mathrm{j},\nabla\Phi_\mathrm{i}\rangle$$

From divergence theorem $\int_\Omega\nabla\cdot\underset{\mathrm{A}}{\rightarrow}\mathrm{d}\Omega=\int_\Gamma\underset{\mathrm{A}}{\rightarrow}\cdot\underset{\mathrm{n}}{\rightarrow}\mathrm{d}\Gamma$

$$\int\nabla\cdot(\nabla\mathrm{u}\cdot\Phi_\mathrm{i})\,\mathrm{d}\Omega=\int\left(\nabla\mathrm{u}\cdot\underset{\mathrm{n}}{\rightarrow}\cdot\Phi_\mathrm{i}\right)\,\mathrm{d}\Gamma$$

Finally,

$$\langle\frac{1}{\mathrm{Re}}\nabla\cdot\left(\nabla\mathrm{u_m}+\mathrm{a_j}\nabla\Phi_\mathrm{j}\right),\Phi_\mathrm{i}\rangle=\frac{1}{\mathrm{Re}}\langle\nabla\mathrm{u_m},\Phi_\mathrm{i}\rangle-\frac{1}{\mathrm{Re}}\langle\nabla\mathrm{u_m},\nabla\Phi_\mathrm{i}\rangle+\mathrm{a_j}\frac{1}{\mathrm{Re}}\langle\nabla\Phi_\mathrm{i},\Phi_\mathrm{i}\rangle-\mathrm{a_j}\frac{1}{\mathrm{Re}}\langle\nabla\Phi_\mathrm{j},\nabla\Phi_\mathrm{i}\rangle$$

ROM representation for the original Navier-Stokes equation are:

$$\mathrm{M}\frac{\partial\mathrm{a}}{\partial\mathrm{t}}=\mathrm{Aa}+\mathrm{a^TQa}+\mathrm{E}\tag{14}$$

$$\mathrm{M}=<\Phi_\mathrm{j},\Phi_\mathrm{i}>\tag{15}$$

$$\mathrm{A}=-<\Phi_\mathrm{j}\cdot\nabla\mathrm{u_m},\Phi_\mathrm{i}>-<\mathrm{u_m}\cdot\nabla\Phi_\mathrm{j},\Phi_\mathrm{i}>-\frac{1}{Re}\langle\nabla\Phi_j,\nabla\Phi_i\rangle-<\nabla\Psi,\Phi_i>+\frac{1}{Re}\langle\nabla\Phi_j,\Phi_i\rangle\tag{16}$$

$$\mathrm{Q}=-<\Phi_j\cdot\nabla\Phi_\mathrm{k},\Phi_\mathrm{i}>\tag{17}$$

$$\mathrm{E}=-<\mathrm{u_m}\cdot\nabla\mathrm{u_m},\Phi_\mathrm{i}>-\langle\nabla\mathrm{p_m},\Phi_\mathrm{i}\rangle+\frac{1}{\mathrm{Re}}\langle\nabla\mathrm{u_m},\Phi_\mathrm{i}\rangle-\frac{1}{\mathrm{Re}}\langle\nabla\mathrm{u_m},\nabla\Phi_\mathrm{i}\rangle\tag{18}$$

1.3 A modified ROM that satisfies both momentum and continuity equations

A modified ROM similar to that proposed in Ref. [2] was implemented and investigated. Derivation of a modified ROM starts from the weak form of Navier Stokes equations:

$$<\mathrm{u_t}+\mathrm{u}\cdot\nabla\mathrm{u}+\nabla\mathrm{p}-\frac{1}{\mathrm{Re}}\nabla\cdot(\nabla\mathrm{u}),\omega_\mathrm{i}>+<\nabla\cdot u,\mathrm{q_i}>=0\tag{19}$$

where ω_i and $\mathrm{q_i}$ belong to appropriate functional spaces. In the current study, $\omega_\mathrm{i}=\Phi_\mathrm{i}$, $\mathrm{q_i}=\alpha(\nabla\cdot\Phi_\mathrm{i})^\mathrm{T}\nabla\cdot\Phi_\mathrm{j}$ are used because this approach gives better results [2]. Additional term is added for the linear term in the Eq.16.

$$\mathrm{A}=-<\Phi_j\cdot\nabla\mathrm{u_m},\Phi_i>-<\mathrm{u_m}\cdot\nabla\Phi_j,\Phi_i>-\frac{1}{Re}\langle\nabla\Phi_j,\nabla\Phi_i\rangle-<\nabla\Psi,\Phi_i>+\frac{1}{Re}\langle\nabla\Phi_i,\Phi_i\rangle+<\alpha\left(\nabla\cdot\Phi_j\right)^T\nabla\cdot\Phi_k,\Phi_i>\tag{20}$$

where the weight α has to be fixed. In this study, we chose $\alpha = 10^{-2}$.

1.4 Stabilization of reduced order models

It is reported that a gradual drifting from the full-state solution to another erroneous state can arise after several vortex shedding periods when ROM equations are integrated in time. It precludes a correct description of the long-term dynamics [3]. What was worse, in some cases, it's hard to use POD ROM as a surrogate model of the original high-fidelity model because the short-term dynamics of the POD ROM may not be sufficiently accurate. For this kind of problem three sources of numerical errors were identified. First, the POD/Galerkin approach can present a lack of inherent numerical stability even for very simple problems [4]. Secondly, the pressure term is often not included in the POD ROM. It is possible to model this term. In current study a pressure extended Reduced Order Model similar to that proposed in Ref. [2] is used. The truncation involved in the POD-Galerkin approach is the third source of instability. Because only small number of POD modes which are the most energetic is kept, the POD ROM is not enough to dissipate the erroneous time amplifications of its solution. For example, 4 modes are sufficient to restore more than 99% of the kinetic energy of the 2D circular cylinder wake flow, but the solution of the such reduced order model does not converge towards the numerical solution of the Navier-Stokes equations [4]. It is thus necessary to stabilize the POD ROM.

It was found that artificial viscosity can help stabilization of POD-Galerkin approach [5]. Adding a constant viscosity acting the same way on all POD modes which is called Heisenberg model [6, 7] is a natural way. In this model, the global dimensionless viscosity 1/Re is thus replaced by another one defined as (1 + c)/Re. In current study, c/Re is used. Then, the next step is to determine or to adjust the constant $c > 0$ in order to obtain a better accuracy for the POD ROM. This concept has been improved by Rempfer and Fasel [8] and Rempfer [9]. They supposed that the dissipation is not identical on each of the POD modes. Thus they replaced the global viscosity with modal viscosities $1/Rei = (1 + c_i)/Re$ on each POD mode. It is then necessary to determine a set of correction coefficients spanned by c_i for $i = 1, \ldots, Nr$.

2. Flow configuration

In this study 2D circular cylinder wake is chosen as a prototype of separated flow. Because this flowfield involves detachments of the boundary layer, wake and vortices interactions with walls, it is interesting. CFD simulation was performed for the experimental condition conducted by Glezer et al. [10], at a Reynolds number (based on the cylinder diameter) of 75500. For this case, a cylinder is placed in the center of an external flow domain. The computational domain size is 32 times the cylinder diameter of 0.0162m. An O-type grid with 257 points in the azimuthal direction and 129 grid points in the normal direction was chosen for the cylinder case (Figure 1). k-w SST turbulence model is used in these studies. The flow is initialized with the free stream conditions. Due to the high Reynolds number of the flow, unsteady flow is observed as expected. Flow separates behind the cylinder and vortex shedding is observed in the wake of the cylinder. Figure 2 shows an instantaneous snapshot of the vortex shedding in the wake of the cylinder. The time-averaged pressure distributions are compared with experimental data in Figure 3. Figure 4 shows time history of lift and drag coefficient. The time-averaged CL,CD, and strouhal number are compared with experiment in Figure 5. The drag coefficient from the CFD, 1.1, is within 3% of the experimental value of 1.07. For the simulation of POD based ROM, the 2D flowfield is extended along spanwise direction. So, there is no variation in velocity and pressure along y-direction.

3. Results of standard reduced order model

Parametric studies were performed in order to investigate the effect of time step, vortex shedding cycle and number of POD modes on the predicted POD coefficients (solution of the ROM). A sampling box of dimensions 0.16 x 0.01 x 0.064 m was chosen as the sub-domain for computing the POD modes. The sampling box was located behind the cylinder. The box encompasses the region where vortex shedding occurs. The test matrix for the parametric studies is shown in Figure 6. The matrix is a combination of time step, scaling factor on Re term and number of POD modes. Figure 7 shows the results of ROM without scaling factor. The temporal evolutions of the predicted mode coefficients are shown in Figure 7.(a). "ODE" means mode coefficient predicted by ROM and "REF" means mode coefficient from POD. Figure 7.(b) shows the comparison of velocity between CFD and POD. "REF" represent velocity from CFD simulation and "POD" is the velocity reconstructed by mode coefficients and shapes. The stability of the ODE generated from ROM is checked by investigating eigenvalues of linear term in Figure 7.(c). The effect of scaling factor is tested in Figure 7 through 9. It is found that the amplitude of modes coefficients decreases by increasing scaling factor. The effect of time step is investigated in Figure 10 through 12 (fixed scaling factor 1500). The first and second mode coefficients shows good agreement with mode coefficient from POD. The amplitudes of third and fourth mode coefficients are underpredicted. It is also found that the divergence of modes coefficient is independent on time step. The effect of number of mode is shown in Figure 12 and 13 because, generally, higher mode shows unstable behavior. For those cases, the scaling factor is also fixed by 1500. The amplitude of mode coefficients predicted by ROM below 6^{th} mode remains within the range. Although the amplitudes over 6^{th} modes are overpredicted it slightly decreases as time increases. It is found that the approach using scaling factor is effective to stabilize the response even for higher modes. Case 8 shows the results with scaling factor of 1300. For this case, the amplitude of all mode coefficients remains almost constant. The nondimensional x-direction velocity (u) reconstructed by ODE is compared with the velocity from POD in Figure 15. The results from ODE shows good agreement with POD.

The effect of numerical scheme on stability of ROM is investigated in Figure 16 through 18. For those cases the scaling factor did not considered. In order to calculate derivatives first order backward, second order central scheme and third order backward scheme are used. Because the first order scheme is dissipative the temporal evolution of mode coefficient shows rapid decrease of amplitude in Figure 16.(a). The solution of ODE using central scheme does not converge (Figure 17). This is because central scheme is less dissipative. The results of third order backward scheme shows diverging behavior (Figure 18). As a next step, the effect of numerical scheme on the magnitude of scaling factor which stabilizes the response of ROM is investigated in Figure 19. It is found that the small scaling factor is needed with higher order scheme. The difference between first and second modes is very small. However, the difference is seen in third and fourth modes between numerical schemes. 5^{th} order scheme shows smaller amplitude than third order scheme. The effect of mesh size used for ROM is tested in Figure 19 and 20. The interesting point is that the results are almost same between third and fifth order scheme even for higher modes. The effect of sampling box size is investigated in Figure 21. Sampling box size of 0.16 x 0.064m was used for above parametric studies. The reduced sampling box (0.0324 m x 0.0324 m) is used for the simulation in Figure 21. It is found that the number of mode required to meet threshold value is increased with reduced sampling box size.

4. Results of pressure extended reduced order model

The pressure term is often not included in the standard POD ROM. Ref. [2] says that absence of pressure term is one of possible reason for instability of POD ROM. It is possible to model this term. In current study a pressure extended Reduced Order Model similar to that proposed in Ref. [2] is derived and

investigated. Simulations were performed for 5 vortex shedding cycles. 51 x 6 x 21 is used as a sample box size. The effect of numerical scheme is investigated in Figure 22. The scaling factor was not applied to these simulations. 2^{nd}, 3^{rd}, 5^{th}, 6^{th} order backward difference schemes are used. The phase difference among numerical schemes are seen. Figure 23 and 24 shows the effect of scaling factor with 5^{th} and 6^{th} order numerical scheme. It is found that the increase of scaling factor stabilizes the response of ROM. Also, another observation is that smaller scaling factor is required with higher order numerical scheme. Figure 25 shows the effect of continuity term on the temporal evolutions of the POD coefficients. 5^{th} order spatial discretization scheme is used for both cases. The scaling factor for Reynolds number is fixed by one. The case without considering of continuity shows rapid increase of amplitude as time goes on. Although both cases show diverging response, the case with continuity term shows more stable behavior. The effect of numerical scheme between second order central and backward scheme is investigated in Figure 26. For these cases the scaling factor of 1300 is used. The central scheme shows slightly rapid decrease of amplitude than backward scheme. Interesting point is found between Figure 25 and 26 for 3^{rd} and 4^{th} modes. Results from 2^{nd} order scheme follows the every peak with phase. However, 5th order does not follow every peak. The effect of scaling factor with 2nd order and 5th order scheme is studied in Figure 27 and 28. As expected, increase of scaling factor reduces the magnitude of amplitude.

5. Results of CFD Ship Airwake of SFS2

The modified ROM including scaling factor was applied to SFS2 case. The SFS model, which was the predecessor to the SFS2, was developed as a result of international collaborative research under The Technical Cooperation Program (TTCP; Ref. [11]). The SFS geometry was proposed in 1996 to create a simple ship model for which a computational grid can easily be built for CFD simulation. The primary aim of these efforts was to enable comparison between different CFD solvers for a simple frigate model. The SFS model is representative of small-size frigates with a superstructure of length 150 ft and a deck of length 90 ft. The nominal height of the superstructure is approximately 35 ft with a small 20 ft projection on the top that represents the communication antennas on a frigate. The SFS model has a uniform width of 45 ft. Later, the updated version of the model, called SFS2, was developed which included an extended superstructure length of 230 ft and bow section of 135 ft at the front for a total length of 455 ft. An unstructured computational grid was generated for the SFS2 which consists of two zones, a near body zone that has a fine mesh to capture the boundary layer and an off body zone that extends to approximately one ship length in both the upstream and downstream directions. The grid consists of 4 million cells made of tetrahedrons in the near body grid and hexahedral cells in the core of the off body grid. The CFD simulations for the SFS2 were performed using OpenFOAM. OpenFOAM is an open source CFD toolbox which is widely used in the fluid dynamics research community. OpenFOAM uses a combination of SIMPLE and PISO algorithms to perform an incompressible unsteady simulation of wind blowing over a stationary ship. Inlet and far field conditions are applied at the upstream and downstream boundaries of the grid, respectively. Slip boundary conditions are used to simulate the water surface. The CFD simulations are run for a WOD speed of 20 m/s at wind azimuths of 0_ and Green 30_ (wind from the starboard side). The simulation is started from ambient conditions and is run for 15 seconds with a nominal time step of 0.006 second. Due to the large grid size, flow-field data was recorded only for the last 10 seconds at a frequency of 0.1 second. The simulations were run in parallel mode on 28 processors.

A sampling boxes of dimensions 108*58*26 ft was chosen as the sub-domain for the simulation of POD based ROM. The sampling box was centered approximately 30 ft aft of the hangar and 20 ft above the deck along the centerline of the ship. The box encompasses the region where a helicopter typically hovers (stationkeeping) before landing on the ship deck. Since the actual ship is not modeled in FLIGHTLAB, the sampling box serves as a representation of the ship deck location. Temporal evolutions

of the predicted POD coefficients and eigenvalues of linear term are shown in Figure 29 for the case without scaling factor on Reynolds number. It was not converged. The "ODE" means the prediction from ROM and "REF" is the mode coefficient from the POD analysis. The real parts of eigenvalues are all positive. The effect of scaling factor is seen in figure 30. The real parts of eigenvalues are negative except 10^{th} and 11^{th} modes. 13 modes are required to meet the threshold requirement. Although the predicted temporal history of mode coefficients are not exactly matched with the mode coefficient from the POD analysis, it shows similar wave form. The effect of numerical scheme is seen between 2nd order (Figure 30) and 5th order (Figure 31). The higher order scheme shows large amplitude than lower order scheme. Figure 32 shows the effect of threshold on temporal evolutions of the POD mode coefficients. The first 5 modes are used. Left figures shows results with 90% threshold and right figures are results of 95% threshold. Overall wave forms are similar between them. There is difference after 8 second. Figure 33 and 34 shows the simulation results with fine sampling box size. Due to the memory limit, large time step is used. The results with 2^{nd} order scheme are seen in Figure 33. In order to check the accuracy of POD analysis the reconstructed velocity at several points are compared with velocity from CFD. The "REF" in Figure33.(b) means the velocity from CFD analysis and "POD" means the velocity reconstructed from the POD analysis. The reconstructed velocity shows good agreement with CFD data. The results with 2^{nd} order scheme are seen in Figure 34.

References

[1] B. R. Noack, P. Papas, P. A. Monkewitz, The need for a pressure-term representation in empirical galerkin models of incompressible shear-flows, J. Fluid Mech. 523 (2005) 339–365**.**

[2] Bergmann, M., Bruneau, C.-H., Iollo, A., Enablers for robust POD models, Journal of Computational Physics, Volume 228, Issue 2, p. 516-538.

[3] S. Sirisup, G. E. Karniadakis, A spectral viscosity method for correcting the long-term behavior of POD model, J. Comp. Phys. 194 (2004) 92–116.

[4] D. Rempfer, On low-dimensional Galerkin models for fluid flow, Theor. Comput. Fluid Dyn. 14 (2000) 75–88.

[5] N. Aubry, P. Holmes, J. L. Lumley, E. Stone, The dynamics of coherent structures in the wall region of a turbulent boundary layer, J. Fluid Mech. 192 (1988) 115–173.

[6] B. Podvin, J. Lumley, A low-dimensional approach for the minimal flow unit, J. Fluid Mech. 362 (1998) 121–151.

[7] J. Delville, L. Ukeiley, L. Cordier, J.-P. Bonnet, M. Glauser, Examination of large-scale structures in a turbulent mixing layer. Part 1. Proper Orthogonal Decomposition, J. Fluid Mech. 391 (1999) 91–122.

[8] D. Rempfer, H. F. Fasel, Evolution of three-dimensional coherent structures in a flat-plate boundary layer, J. Fluid Mech. 260 (1994) 351–375.

[9] D. Rempfer, Investigations of boundary layer transition via Galerkin Projections on Empirical Eigenfunctions, Phys. Fluids 8 (1) (1996) 175–188.

[10] Glezer, A., Amitay, M. and Honohan, A. M., "Aspects of Low- and High-Frequency Actuation for Aerodynamic Control," *AIAA Journal*, Vol. 43, No. 7, July 2005.

[11] Hodge, S. J., Zan, S. J., Roper, D. M., Padfield, G. D., and Owen, I., "Time-Accurate Ship Airwake and Unsteady Aerodynamic Loads Modeling for Maritime Helicopter Simulation," Journal of the American Helicopter Society, Vol. 54, No. 1, January 2009, pp. 022005–1–022005–16.

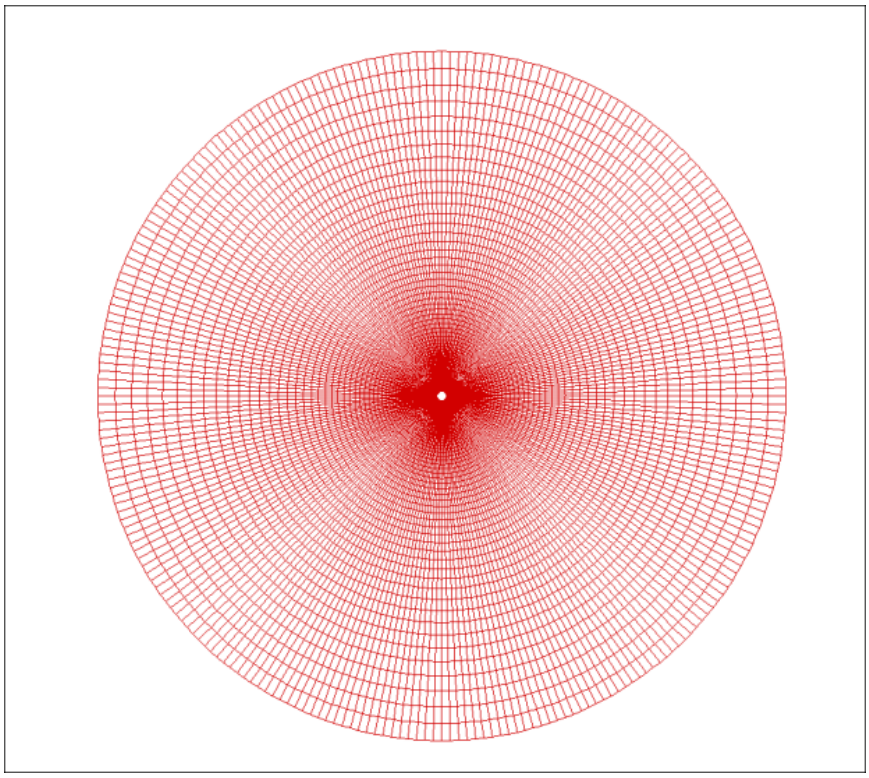

Figure 1: 2D circular cylinder computational grid

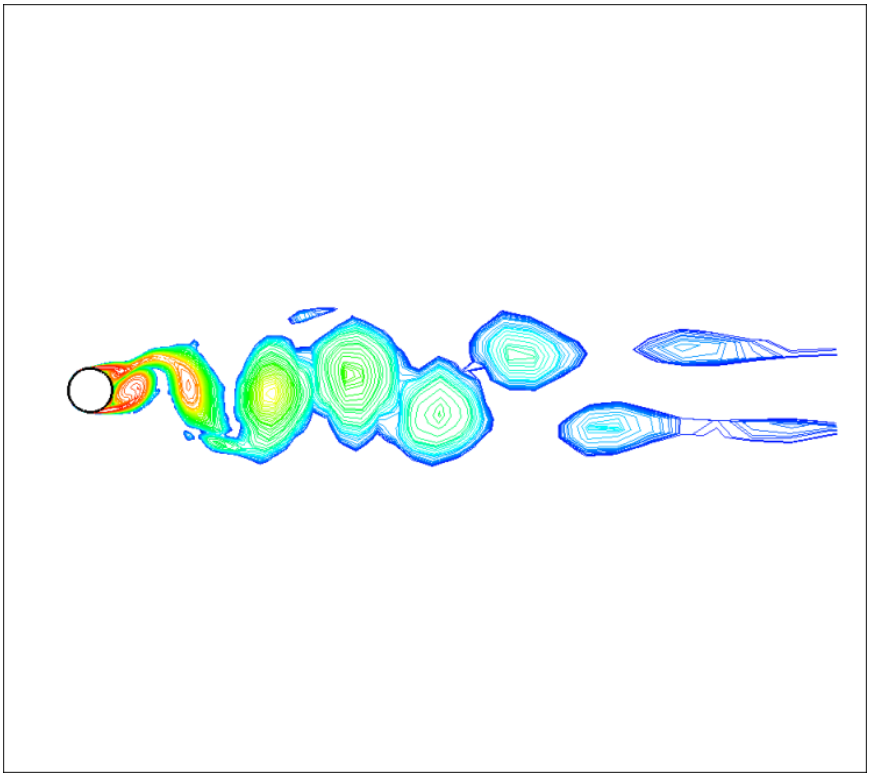

Figure 2: Instantaneous vorticity behind the cylinder at Re = 75500

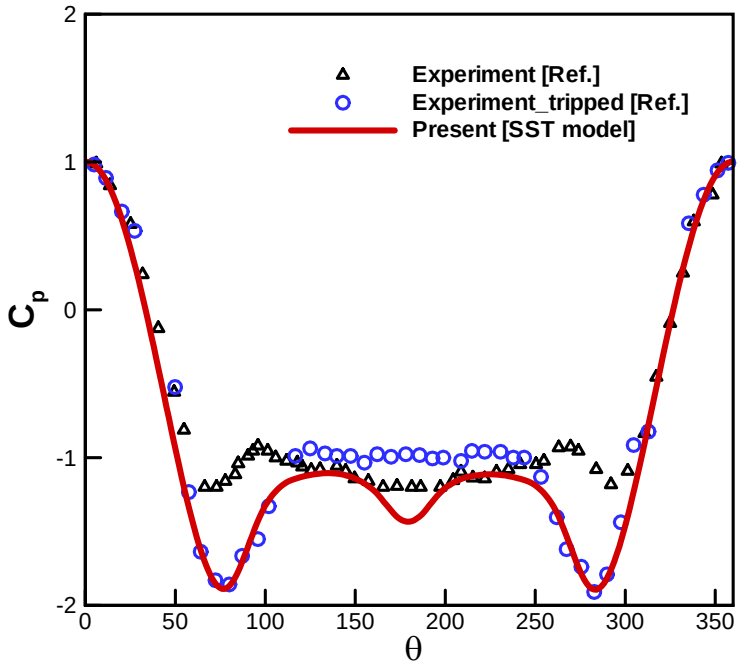

Figure 3: Comparison of Cp between experiment and two-dimensional simulation.

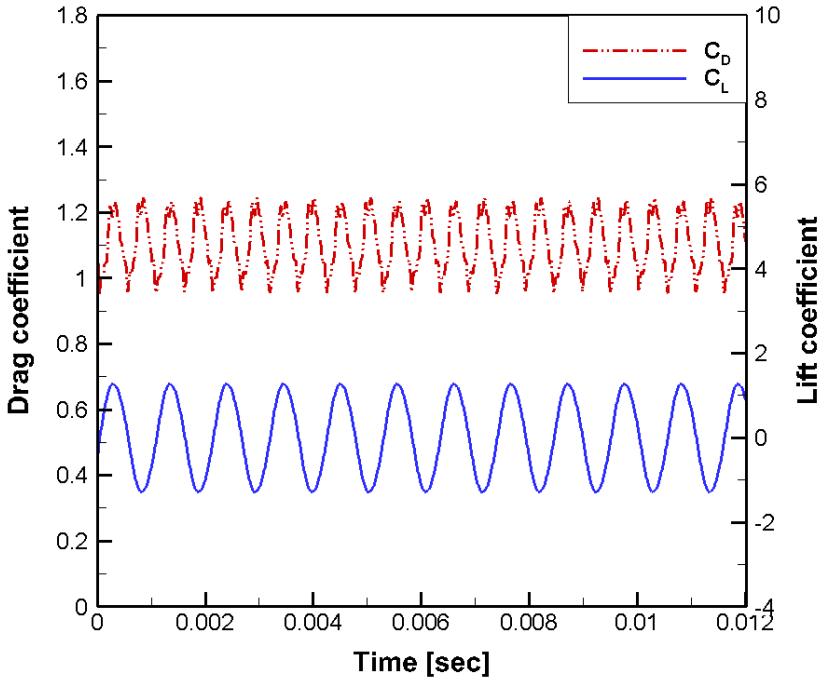

Figure 4: Time history of lift and drag coefficient.

- Force coefficient

	CL	CD
Experiment	**0.0**	**1.07 (CD_{press})**
CFD (present)	**0.0**	**1.1 (CD_{press} +CD_{visc})**

- Strouhal number

	Strouhal number
Experiment	**0.21**
CFD (present)	**0.227**

Figure 5: Comparison of CL,CD, and Strouhal number with experiment.

Case	Factor	Number of POD modes	Time step for POD	Cycle for vortex shedding	Convergence of ODE
1	1	4	4.76189E-06 sec	1	O
2	1500	4	4.76189E-06 sec	1	O
3	2000	4	4.76189E-06 sec	1	O
4	1500	4	9.52379E-06 sec	2	O
5	1500	4	1.42857E-05sec	3	O
6	1500	4	2.38E-05 sec	5	O
7	1500	10	2.38E-05 sec	5	O
8	1300	10	2.38E-05 sec	5	O

Figure 6: Test matrix for 2D cylinder parametric studies.

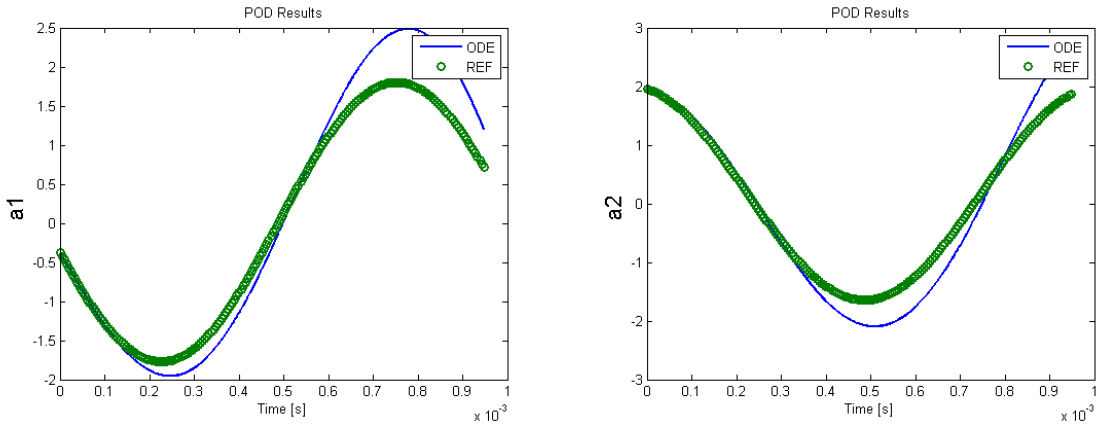

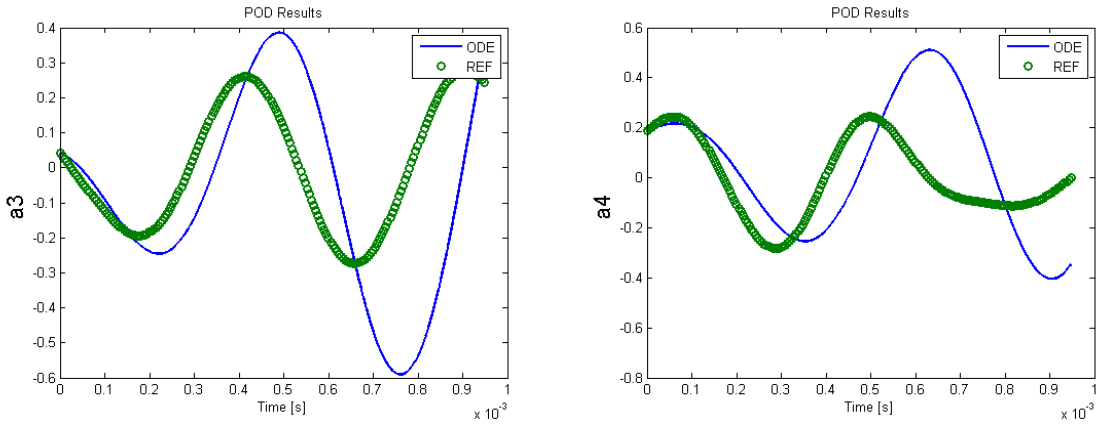

(a) Temporal evolutions of the predicted POD coefficients

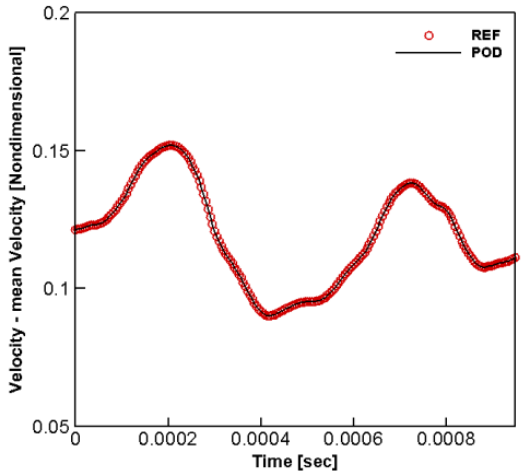

(b) Comparison of velocity between CFD and POD analysis

Mode	Eigenvalue
1	0.1091 + 1.3729i
2	0.1091 - 1.3729i
3	0.1083 + 1.6117i
4	0.1083 - 1.6117i

(c) Stability check : eigenvalues of linear term

Figure 7: Parametric study results (case 1).

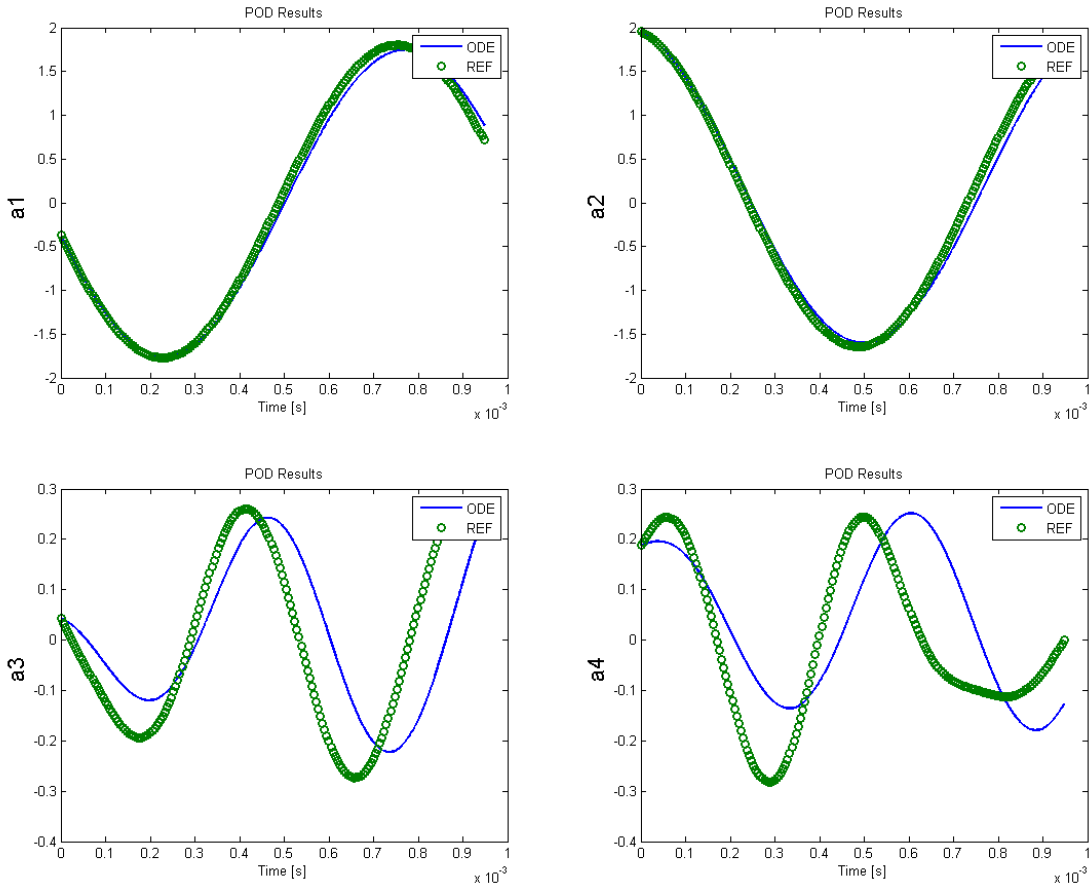

(a) Temporal evolutions of the predicted POD coefficients

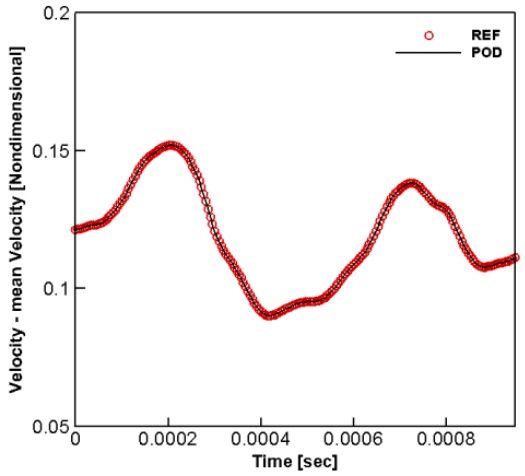

(b) Comparison of velocity between CFD and POD analysis

Mode	Eigenvalue
1	-0.0023 + 1.3778i
2	-0.0023 - 1.3778i
3	-0.3511 + 1.6086i
4	-0.3511 - 1.6086i

(c) Stability check : eigenvalues of linear term

Figure 8: Parametric study results (case 2).

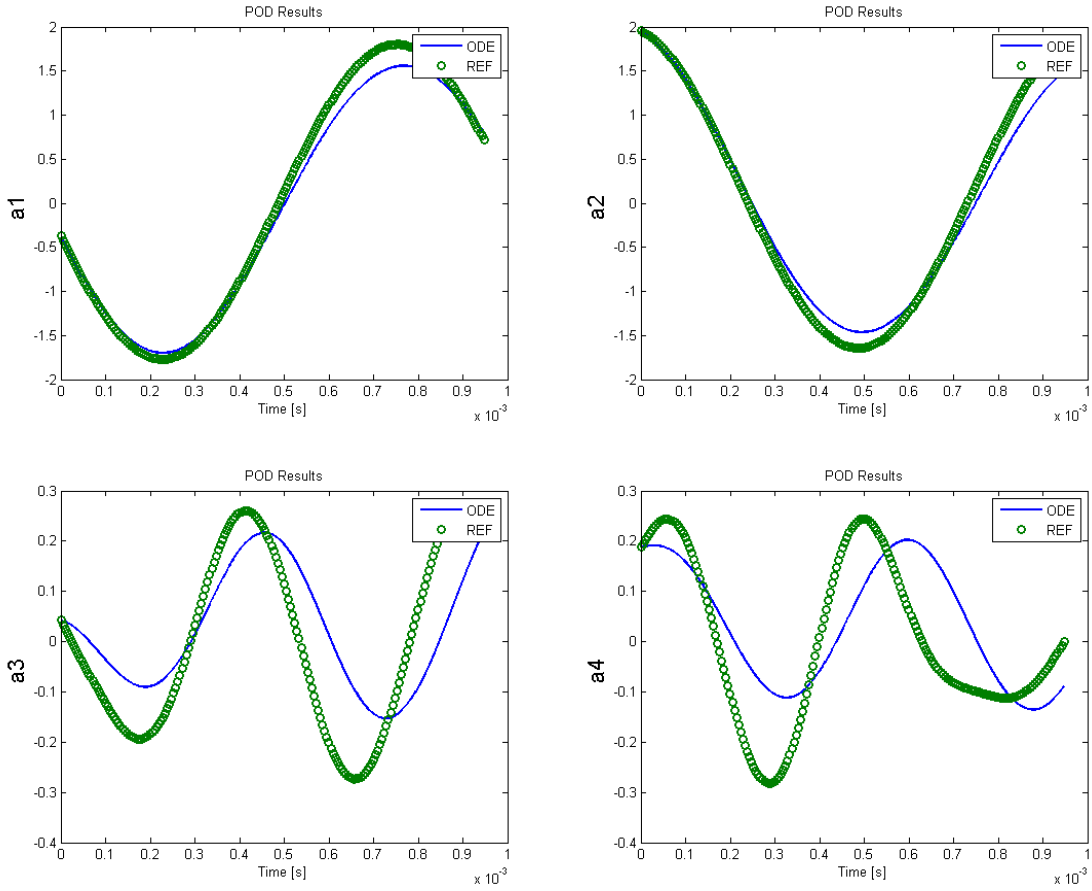

(a) Temporal evolutions of the predicted POD coefficients

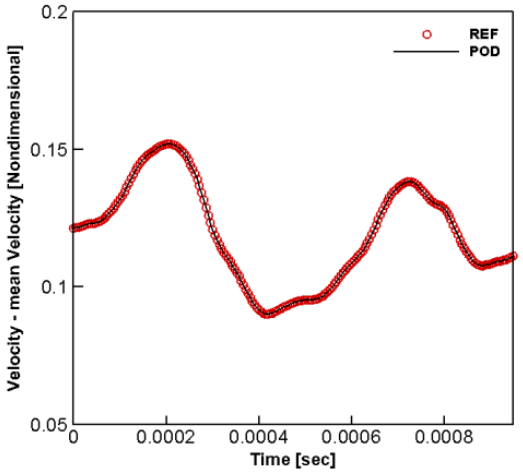

(b) Comparison of velocity between CFD and POD analysis

Mode	Eigenvalue
1	-0.0389 + 1.3782i
2	-0.0389 - 1.3782i
3	-0.5050 + 1.6087i
4	-0.5050 - 1.6087i

(c) Stability check : eigenvalues of linear term

Figure 9: Parametric study results (case 3).

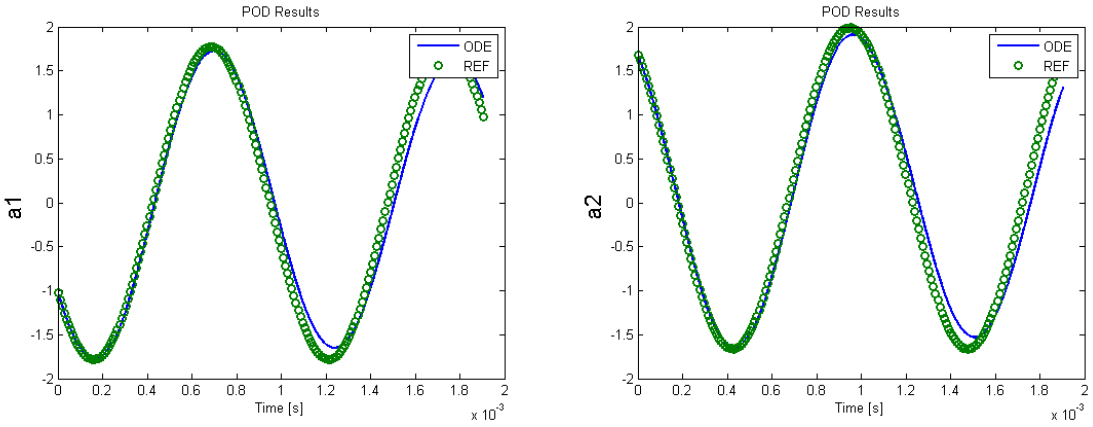

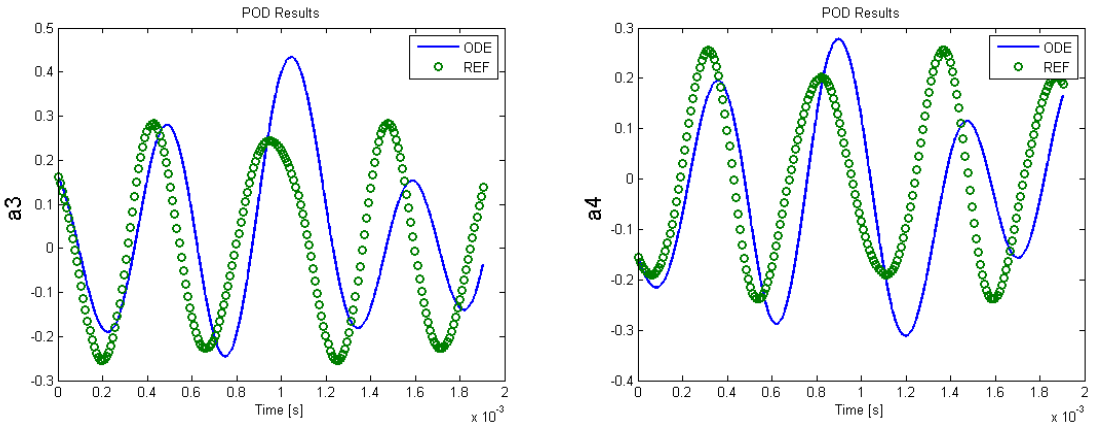

(a) Temporal evolutions of the predicted POD coefficients

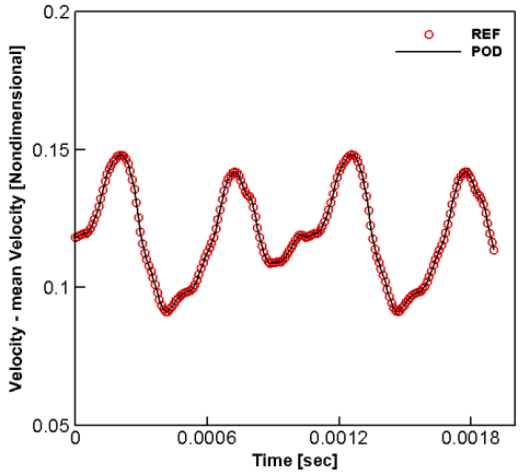

(b) Comparison of velocity between CFD and POD analysis

Mode	Eigenvalue
1	-0.0016 + 1.3783i
2	-0.0016 - 1.3783i
3	-0.3573 + 1.8949i
4	-0.3573 - 1.8949i

(c) Stability check : eigenvalues of linear term

Figure 10: Parametric study results (case 4).

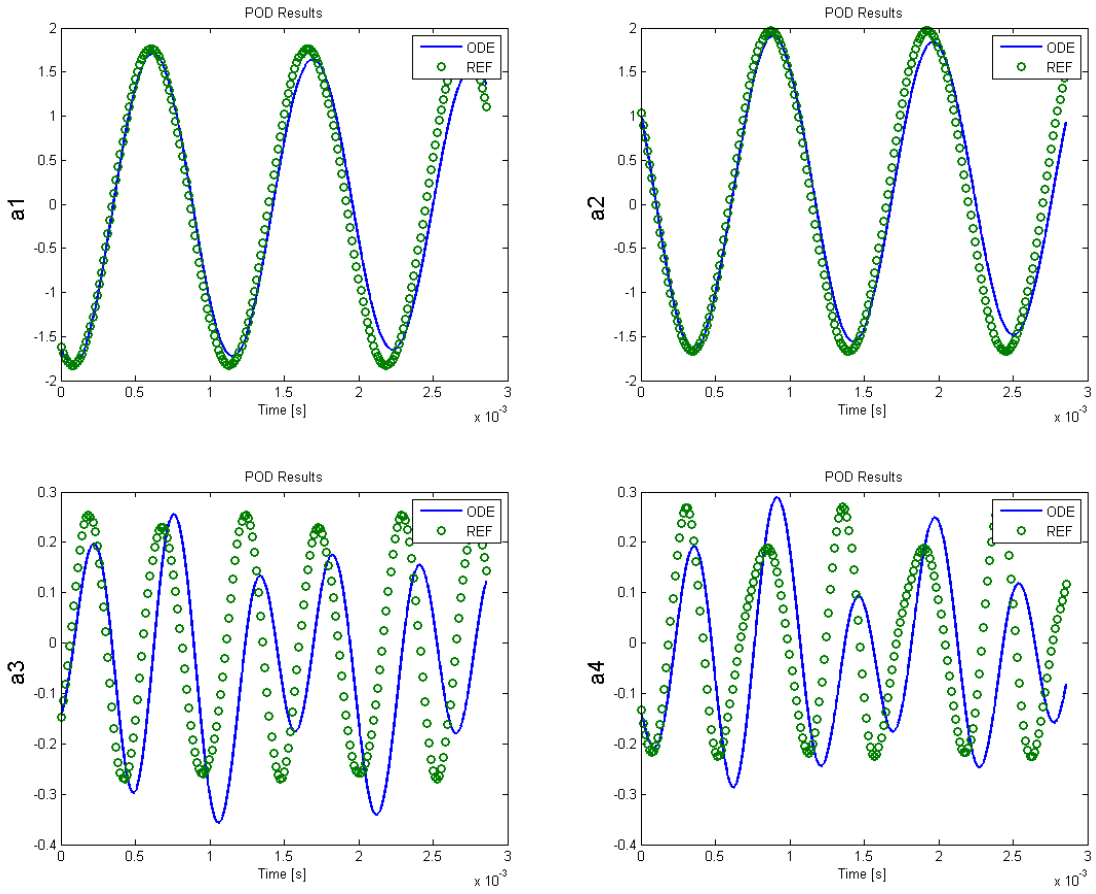

(a) Temporal evolutions of the predicted POD coefficients

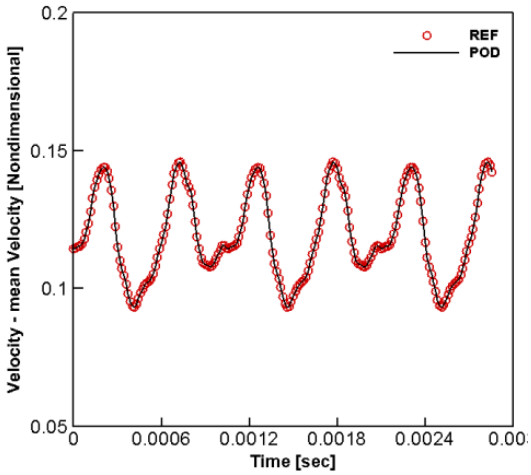

(b) Comparison of velocity between CFD and POD analysis

Mode	Eigenvalue
1	-0.0007 + 1.3794i
2	-0.0007 - 1.3794i
3	-0.3580 + 1.8518i
4	-0.3580 - 1.8518i

(c) Stability check : eigenvalues of linear term

Figure 11: Parametric study results (case 5).

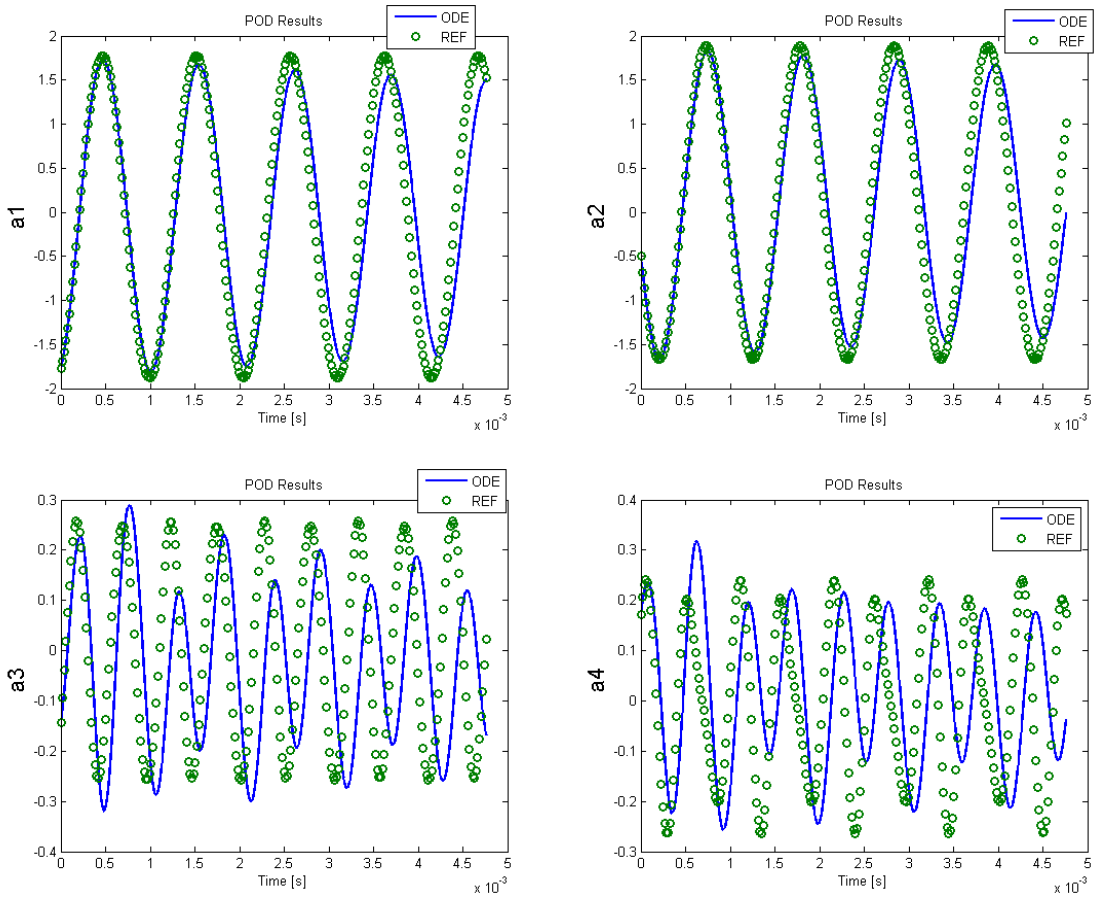

(a) Temporal evolutions of the predicted POD coefficients

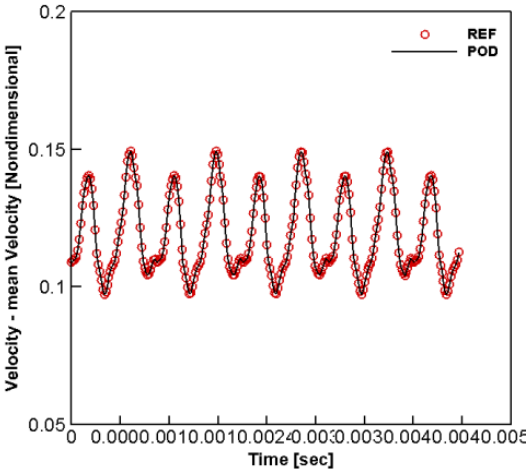

(b) Comparison of velocity between CFD and POD analysis

Mode	Eigenvalue
1	-0.0002 + 1.3784i
2	-0.0002 - 1.3784i
3	-0.3524 + 1.8356i
4	-0.3524 - 1.8356i

(c) Stability check : eigenvalues of linear term

Figure 12: Parametric study results (case 6).

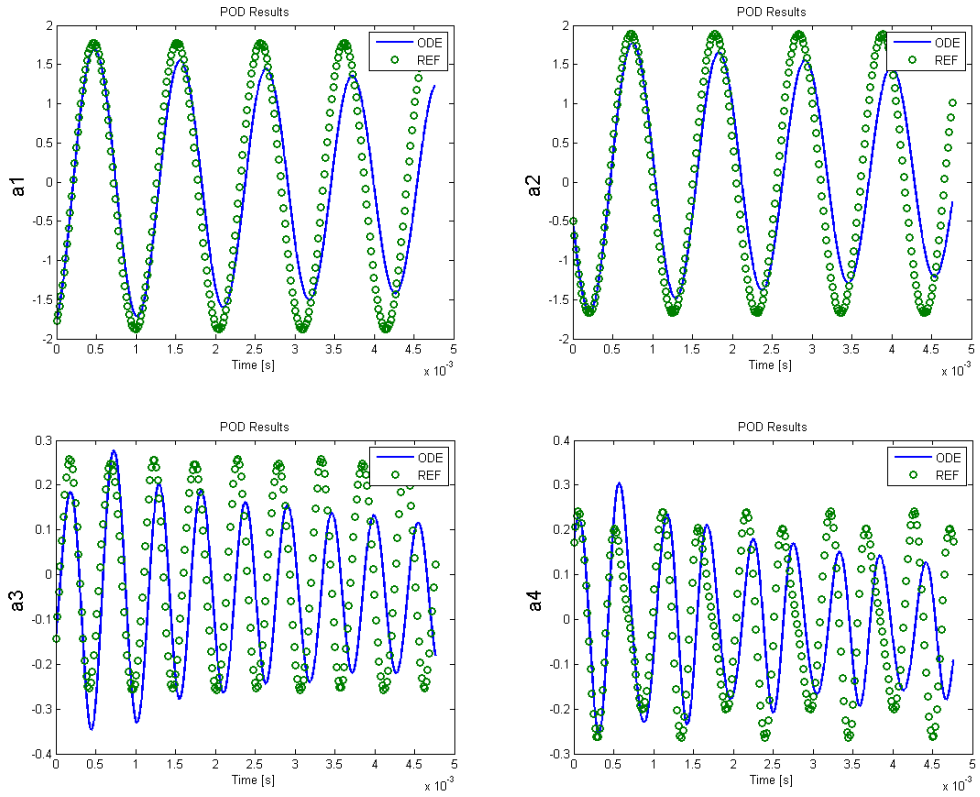

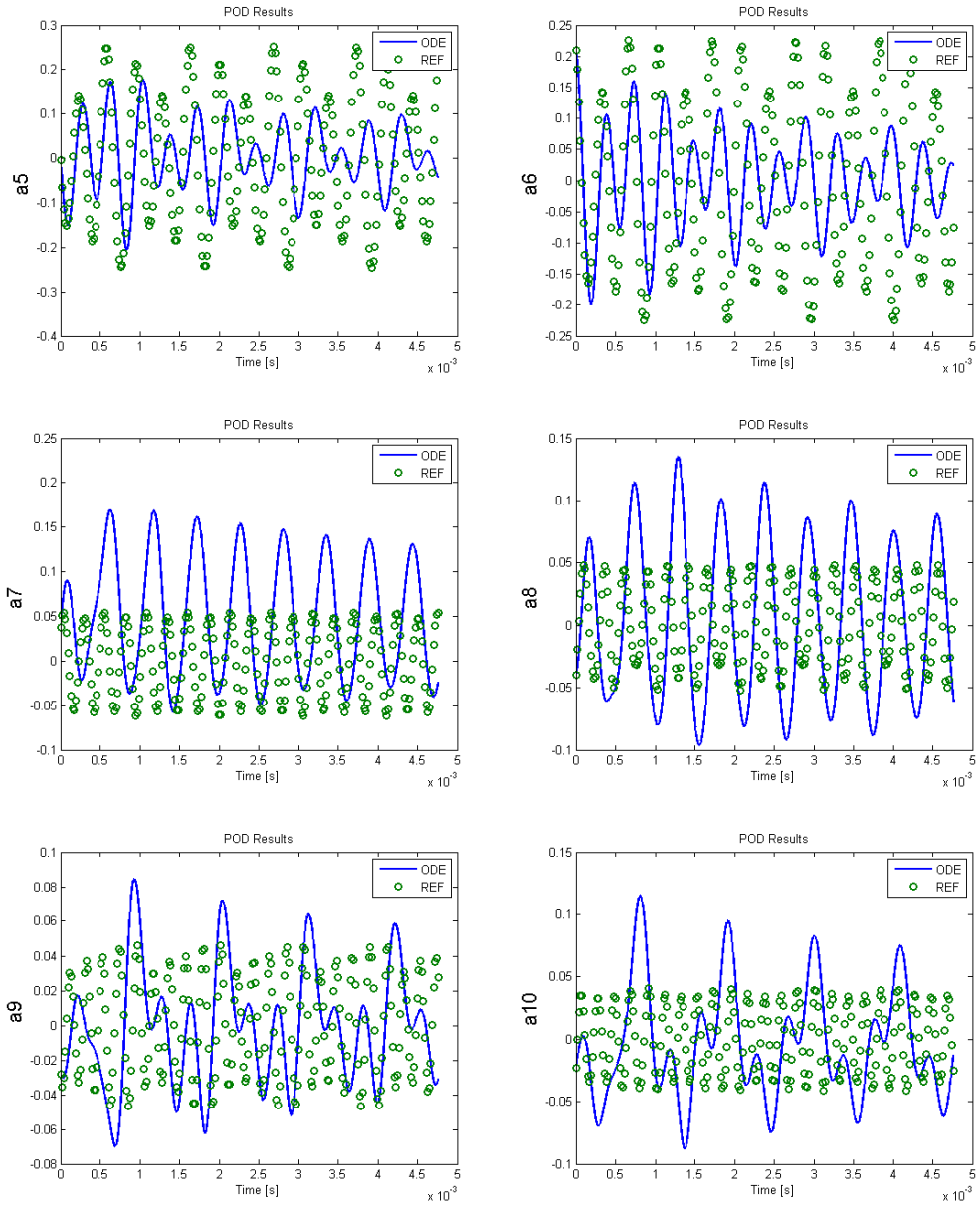

(a) Temporal evolutions of the predicted POD coefficients

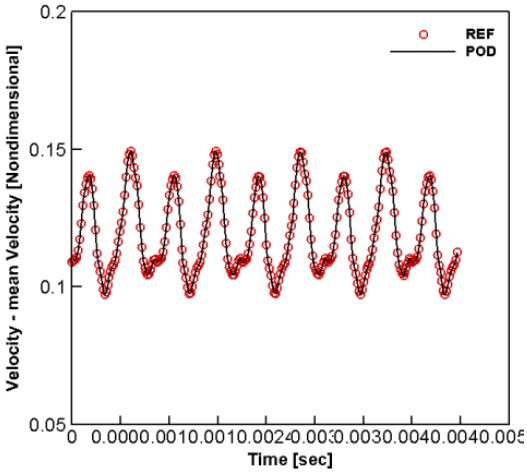

(b) Comparison of velocity between CFD and POD analysis

-Stability check : eigenvalues of linear term

Mode	Eigenvalue
1	-0.0015 + 1.3768i
2	-0.0015 - 1.3768i
3	-0.4542 + 1.6901i
4	-0.4542 - 1.6901i
5	-0.4770 + 3.2011i
6	-0.4770 - 3.2011i
7	-0.5179 + 2.8226i
8	-0.5179 - 2.8226i
9	-0.4758 + 2.6528i
10	-0.4758 - 2.6528i

(c) Stability check : eigenvalues of linear term

Figure 13: Parametric study results (case 7).

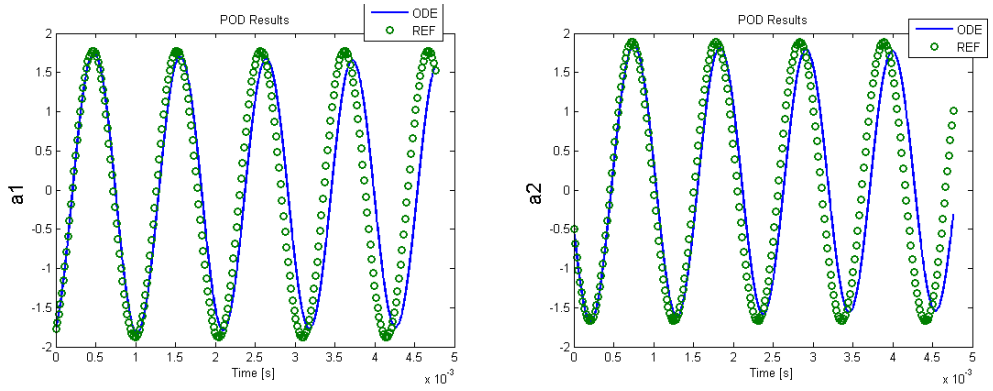

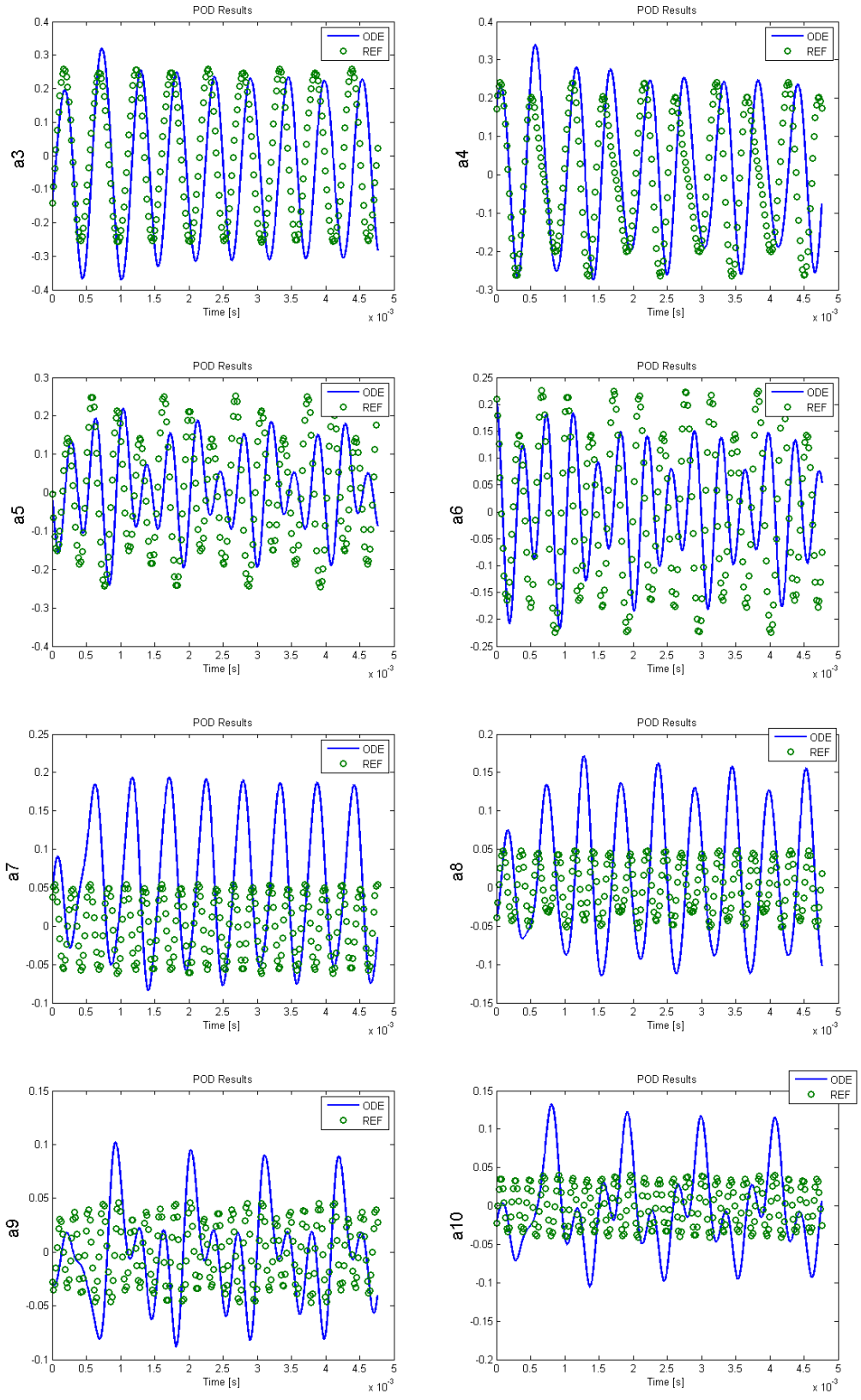

(a) Temporal evolutions of the predicted POD coefficients

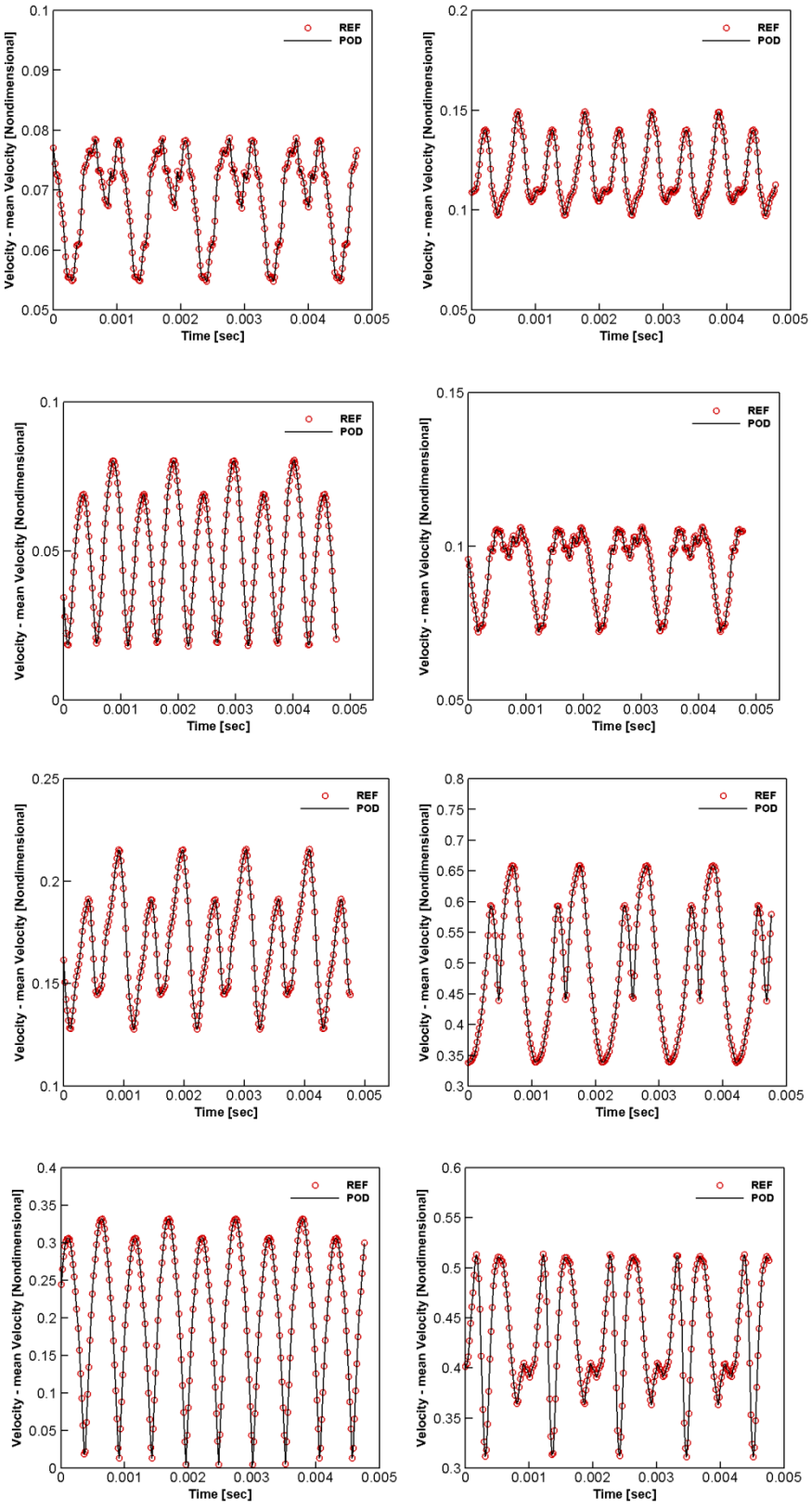

(b) Comparison of velocity between CFD and POD analysis

Mode	Eigenvalue
1	0.0134 + 1.3766i
2	0.0134 - 1.3766i
3	-0.3862 + 1.6855i
4	-0.3862 - 1.6855i
5	-0.4094 + 3.2057i
6	-0.4094 - 3.2057i
7	-0.4388 + 2.8186i
8	-0.4388 - 2.8186i
9	-0.3957 + 2.6568i
10	-0.3957 - 2.6568i

(c) Stability check : eigenvalues of linear term

Figure 14: Parametric study results (case 8).

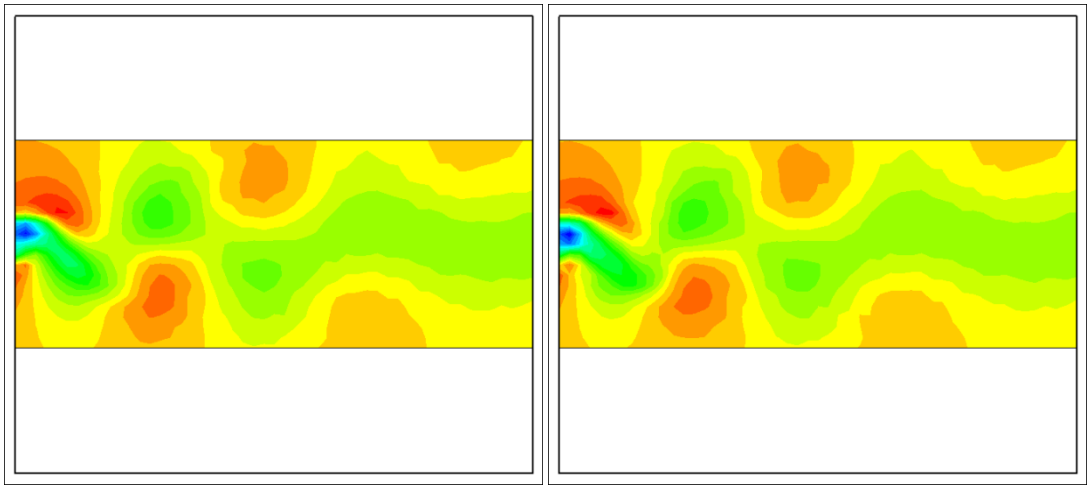

< t = 0 >

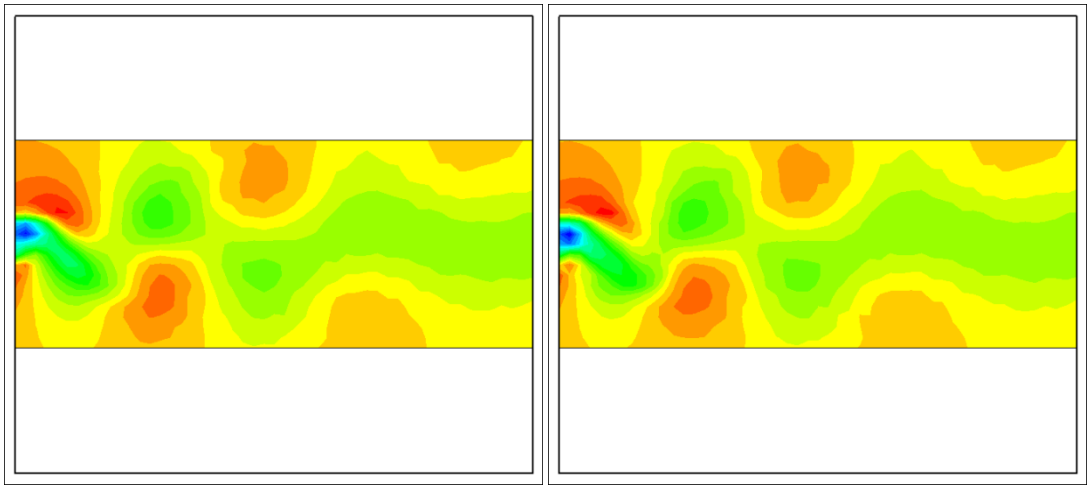

< t = 0.1 T >

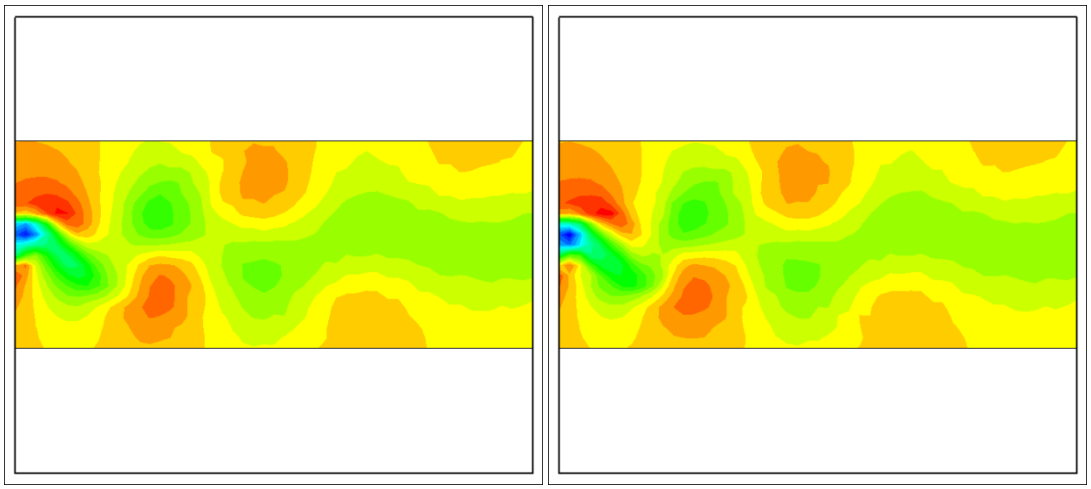

< t = 0.2 T >

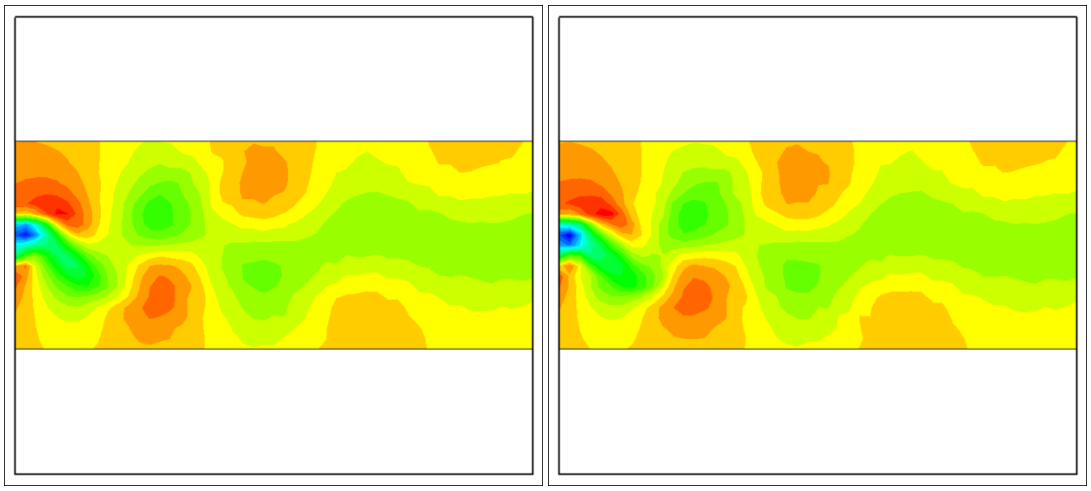

< t = 0.3 T >

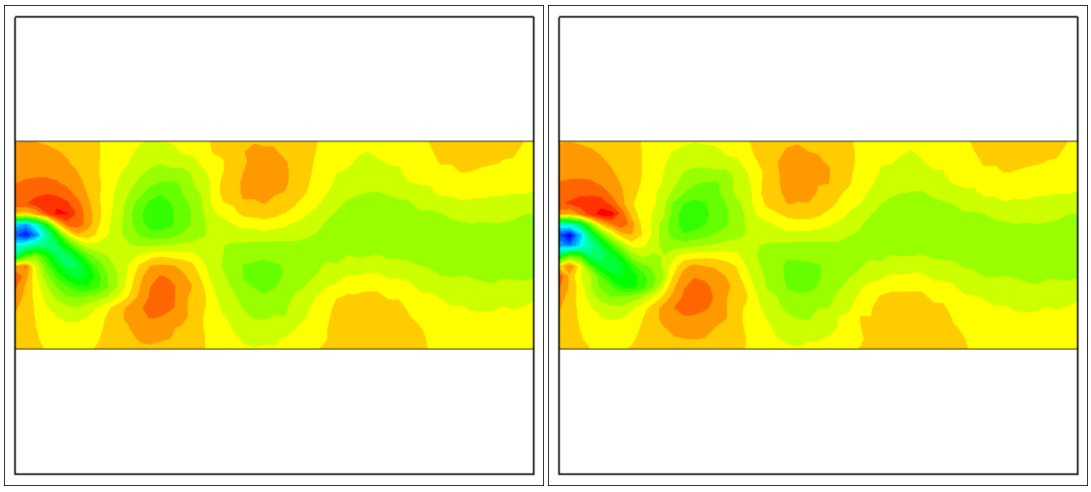

< t = 0.4 T >

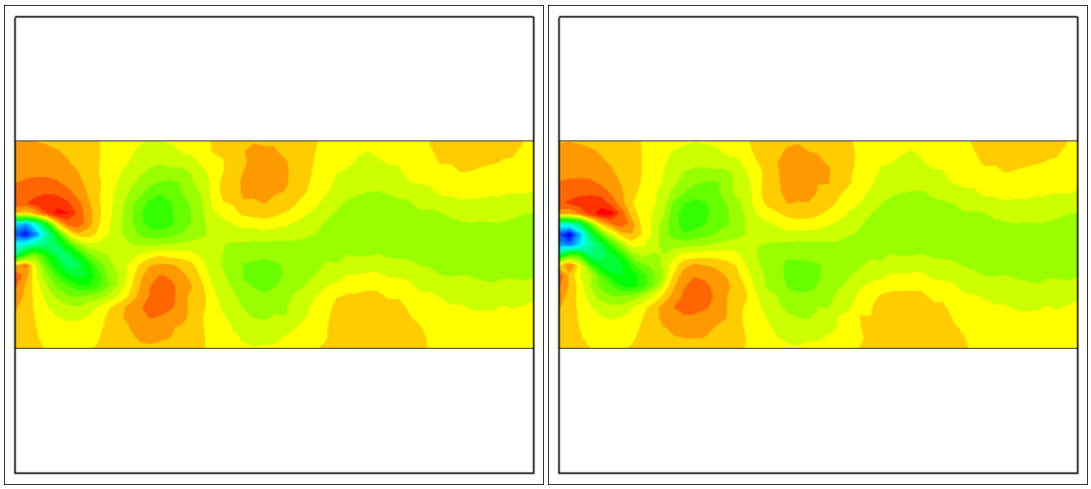

< t = 0.5 T >

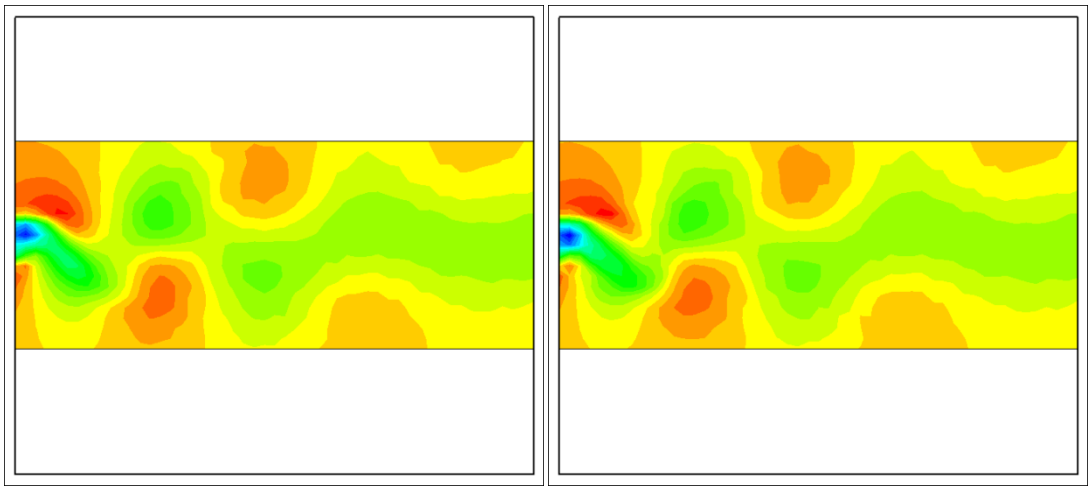

< t = 0.6 T >

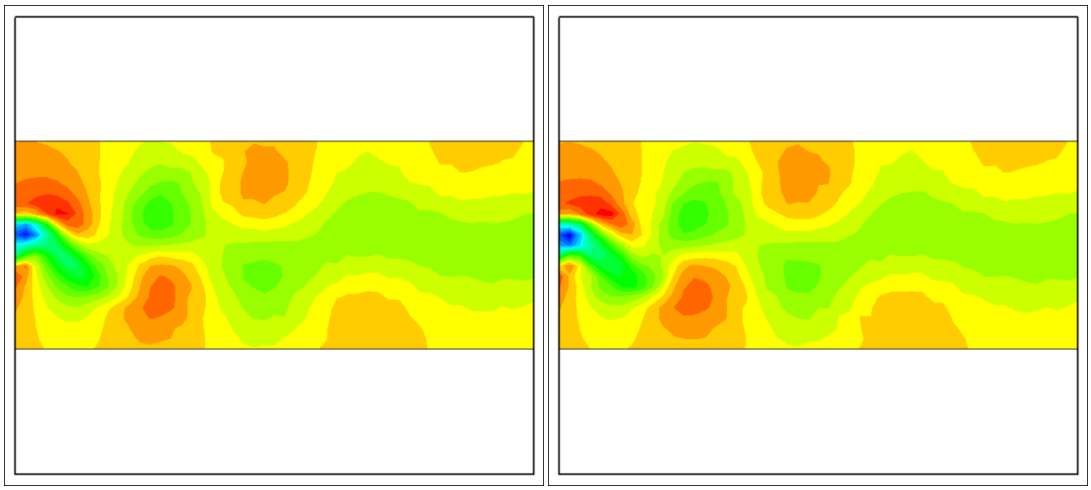

< t = 0.7 T >

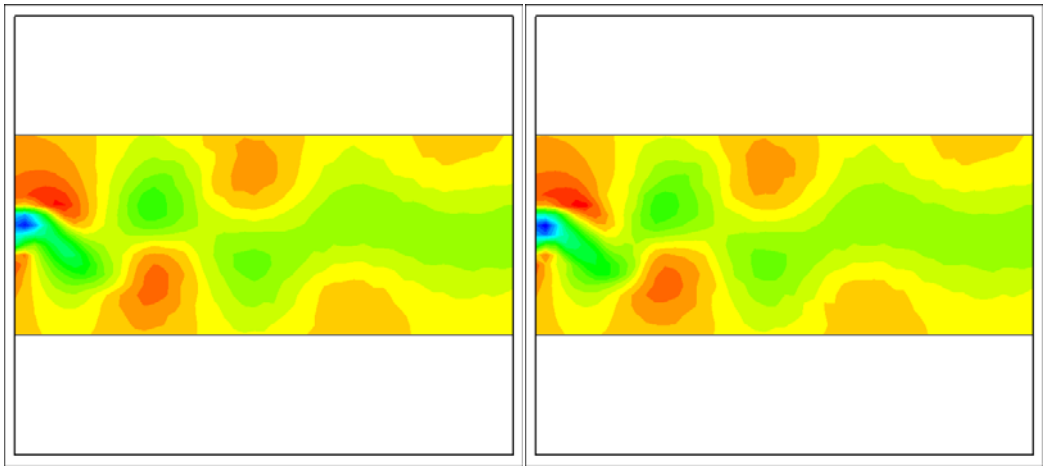

< t = 0.8 T >

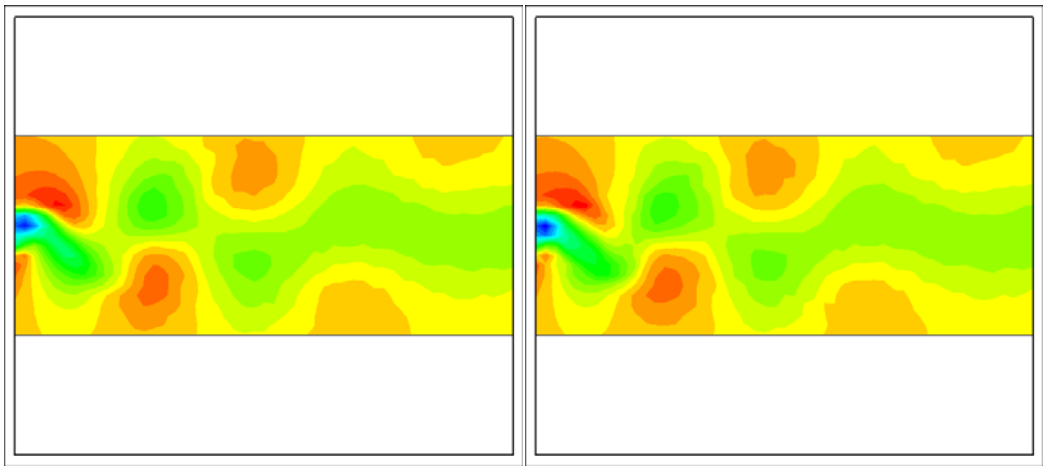

< t = 0.9 T >

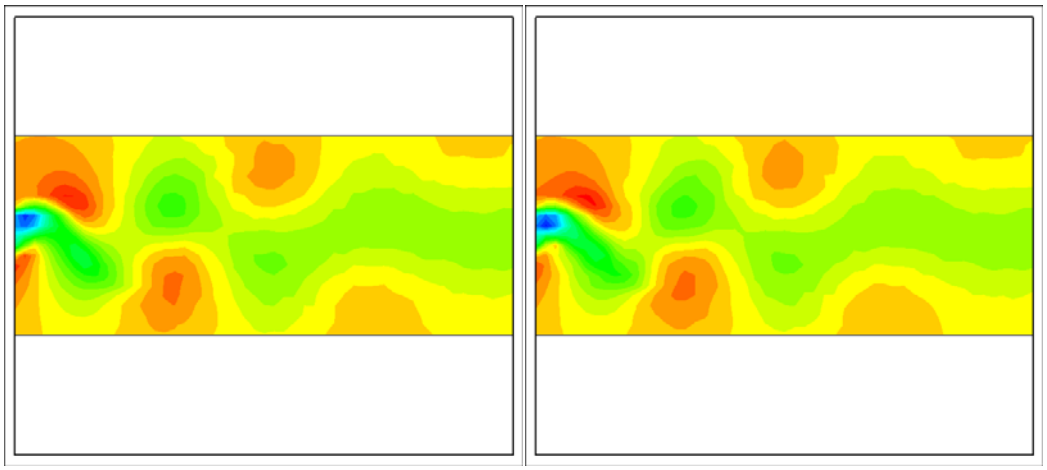

< t = T >

Figure 15: Comparison of nondimensional u velocity (Left : POD, Right : ODE).

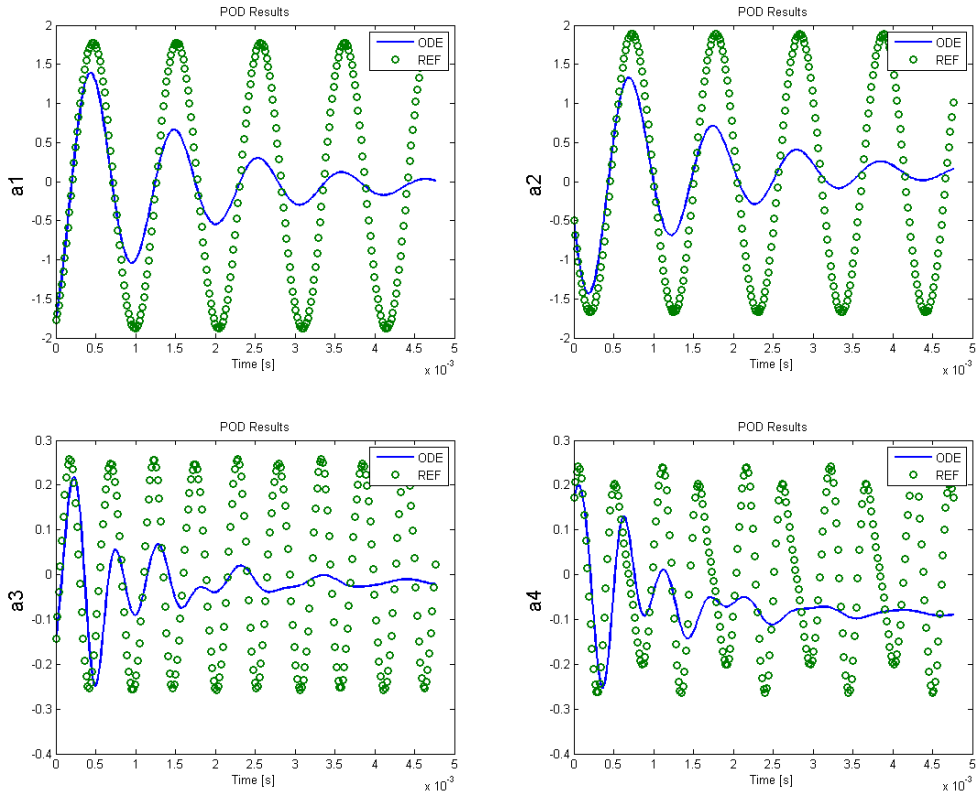

(a) Temporal evolutions of the predicted POD coefficients

Mode	Eigenvalue
1	-0.1624 + 1.4255i
2	-0.1624 - 1.4255i
3	-0.7129 + 1.9308i
4	-0.7129 + 1.9308i

(b) Stability check : eigenvalues of linear term

Figure 16 : ROM results with first order spatial discretization scheme.

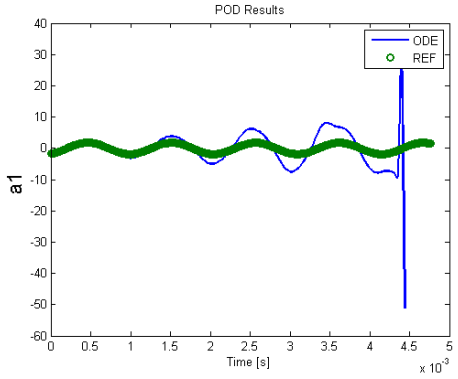

(a) Temporal evolutions of the predicted POD coefficients

Mode	Eigenvalue
1	0.1183 + 1.3851i
2	0.1183 - 1.3851i
3	0.0821 + 1.8470i
4	0.0821 - 1.8470i

(b) Stability check : eigenvalues of linear term

Figure 17 : ROM results with second order central spatial discretization scheme.

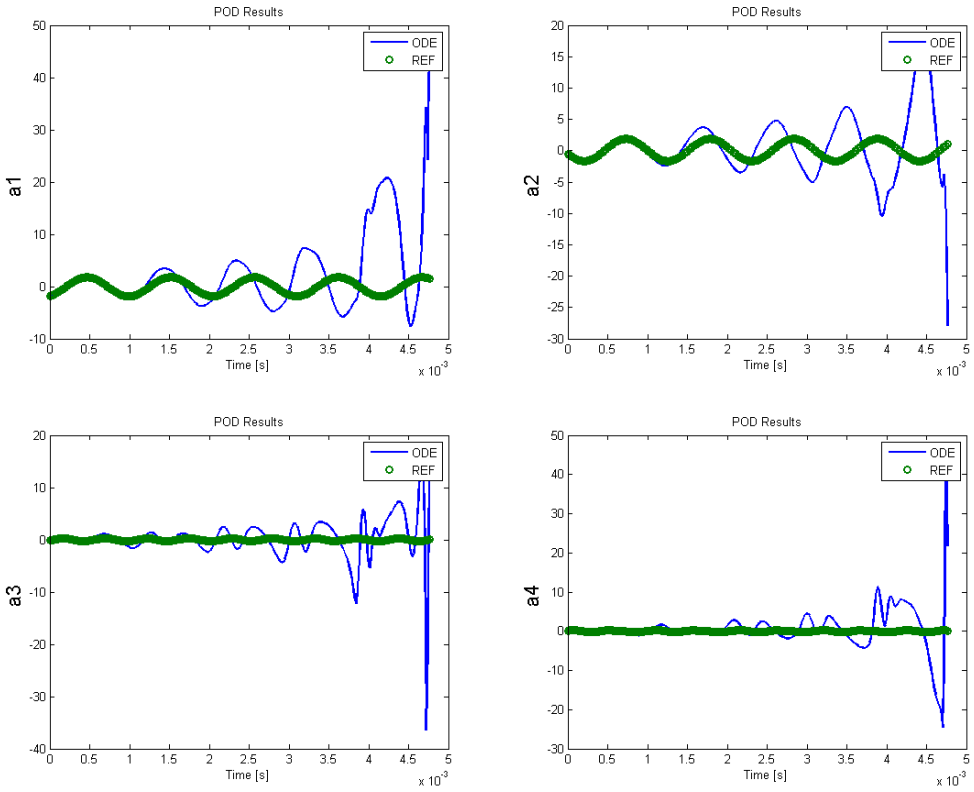

(a) Temporal evolutions of the predicted POD coefficients

Mode	Eigenvalue
1	0.1037 + 1.4062i
2	0.1037 - 1.4062i
3	0.0499 + 2.2578i
4	0.0499 - 2.2578i

(b) Stability check : eigenvalues of linear term

Figure 18 : ROM results with third order backward spatial discretization scheme

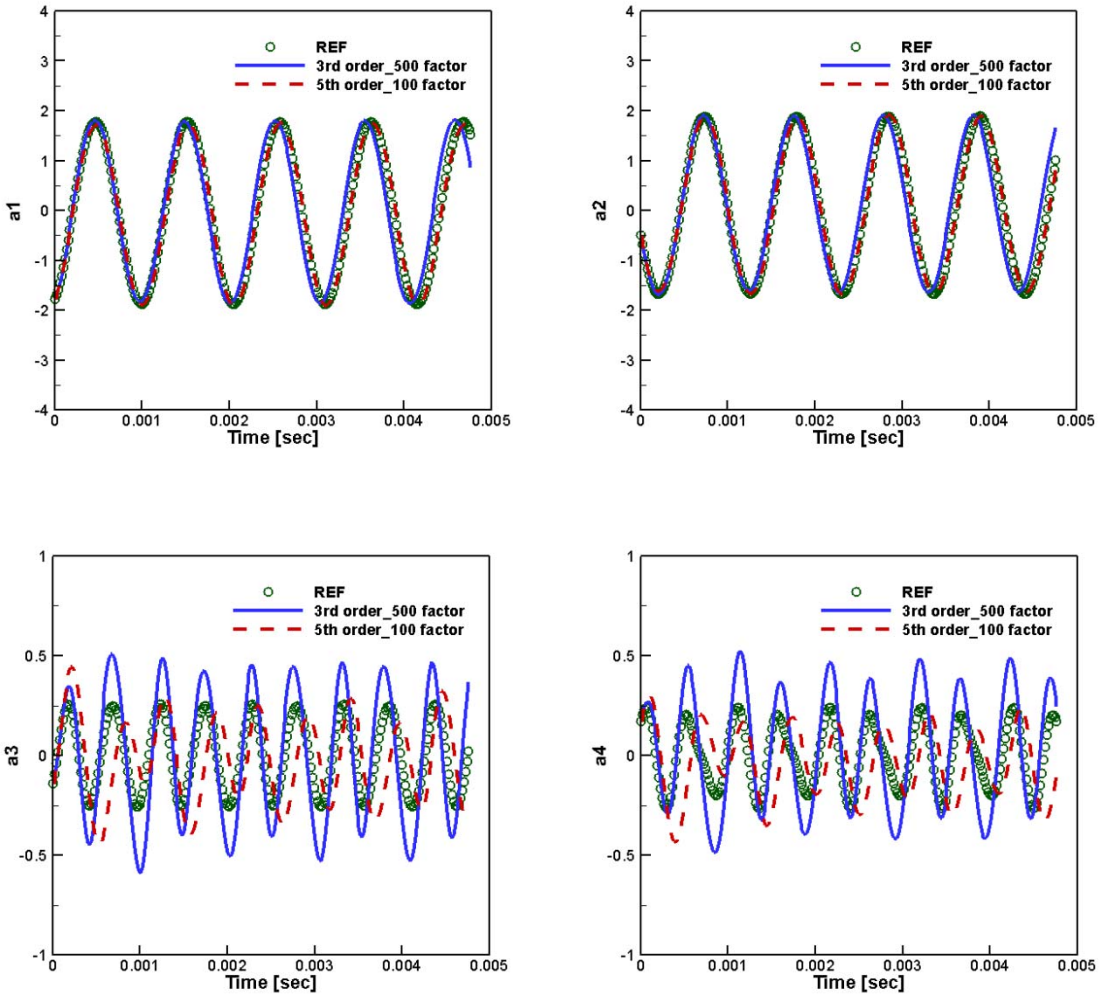

Figure 19: Comparison between third and fifth order (sample box size : 51 x 6 x 21, Time step: 2.38E-05 sec, cycle for vortex shedding:5)

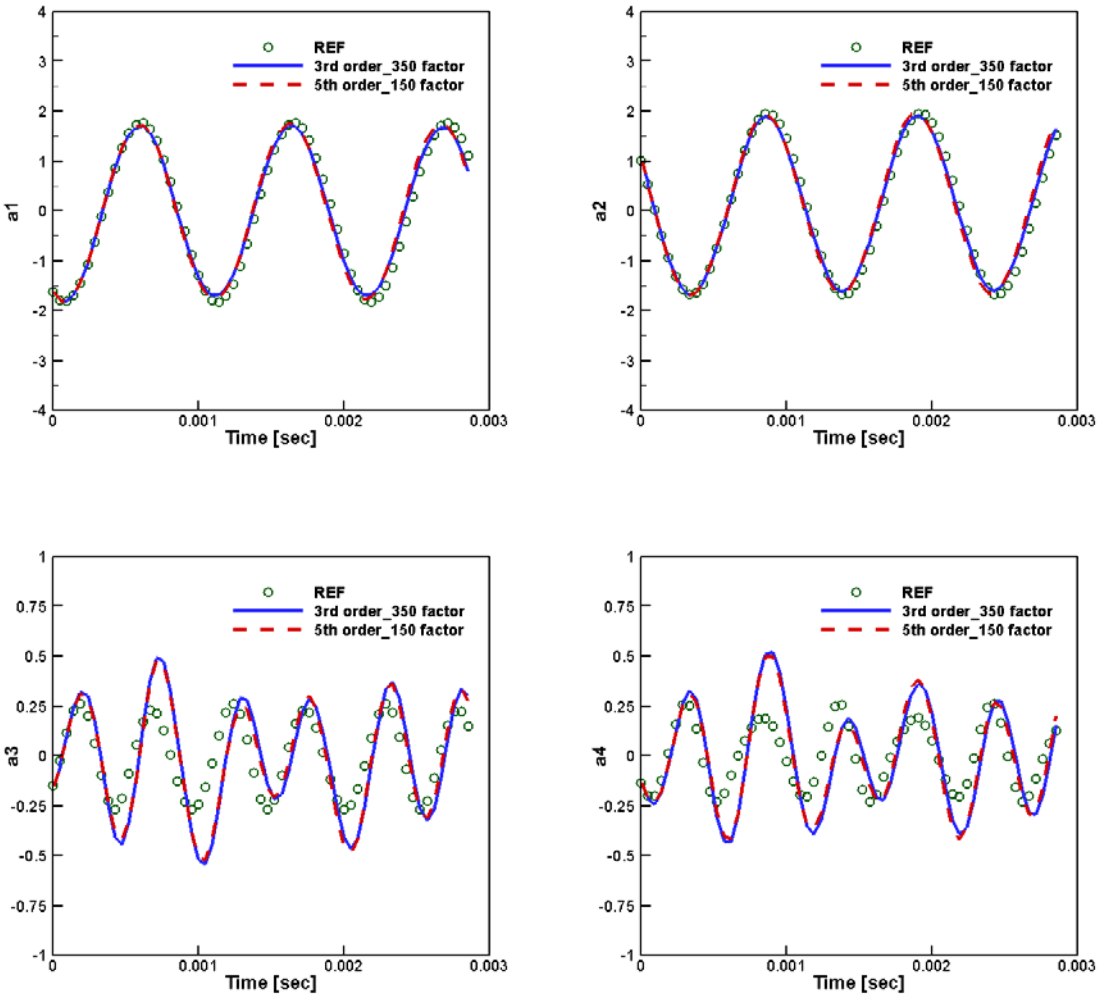

Figure 20: Comparison between third and fifth order (sample box size : 109 x 12 x 45, Time step: 4.76E-5 sec, cycle for vortex shedding:3)

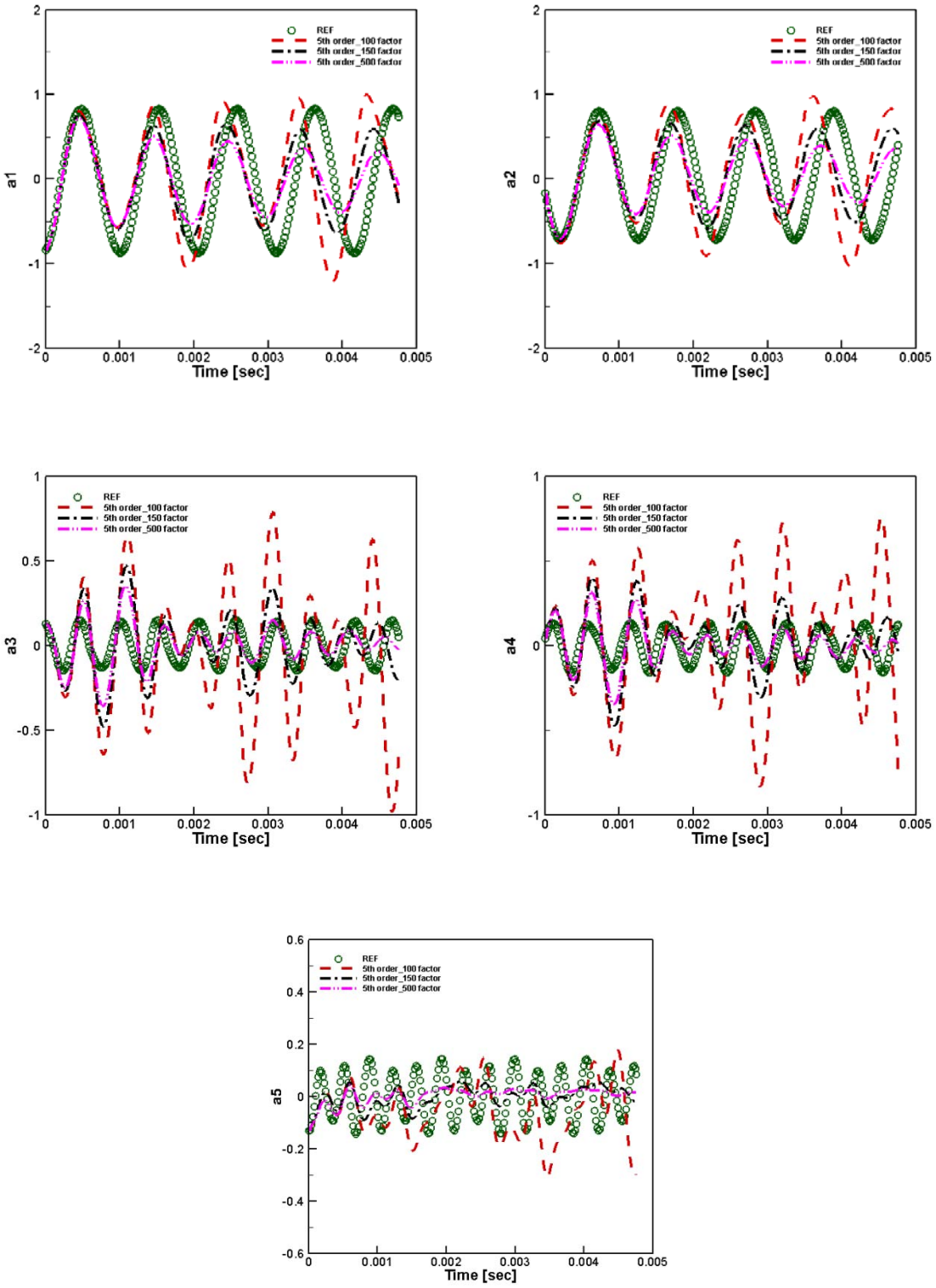

Figure 21: Effect of scaling factor (sample box size : 0.0324 m x 0.0324 m, Time step: 2.38E-05 sec, cycle for vortex shedding:5)

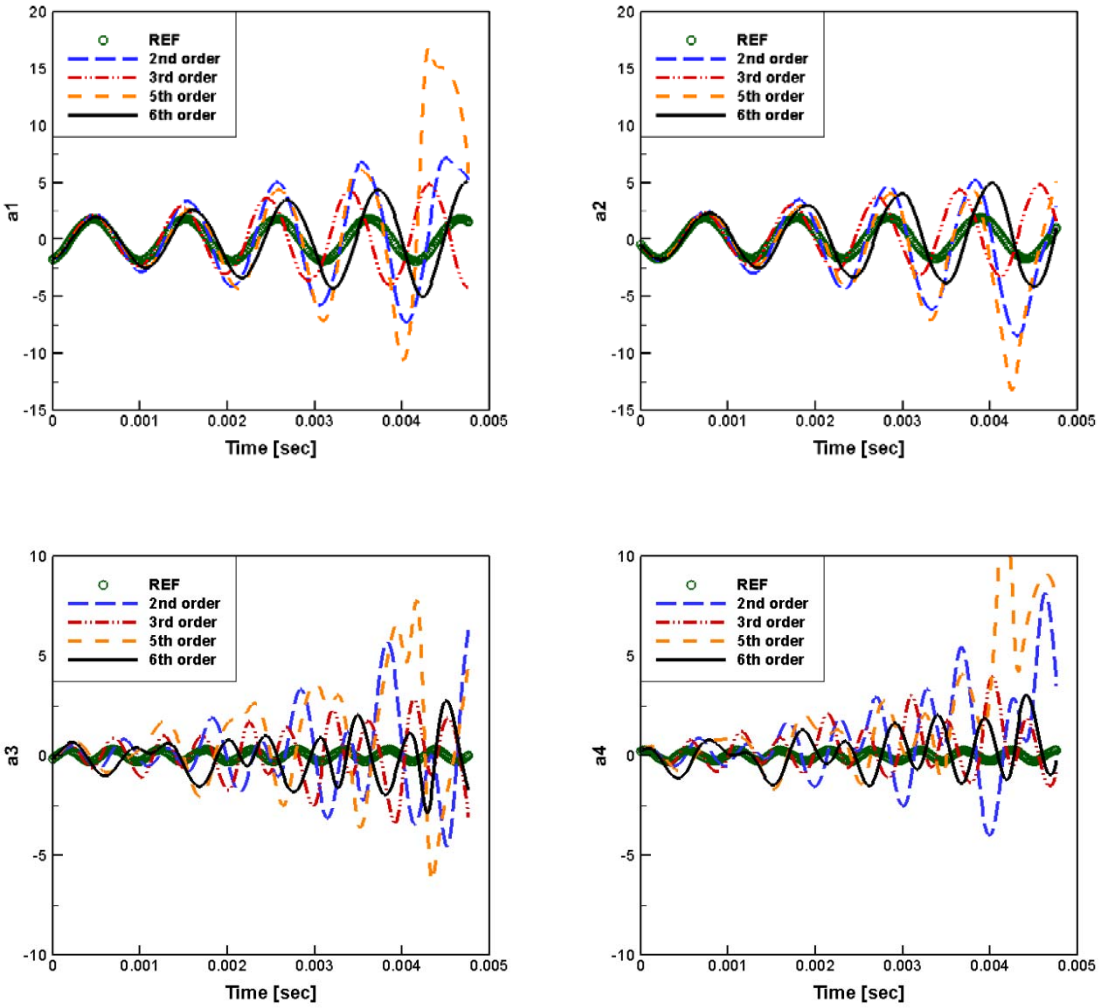

Figure 22: Effect of numerical scheme with a pressure extended ROM (sample box size : 51 x 6 x 21, Time step: 2.38E-05 sec, cycle for vortex shedding:5)

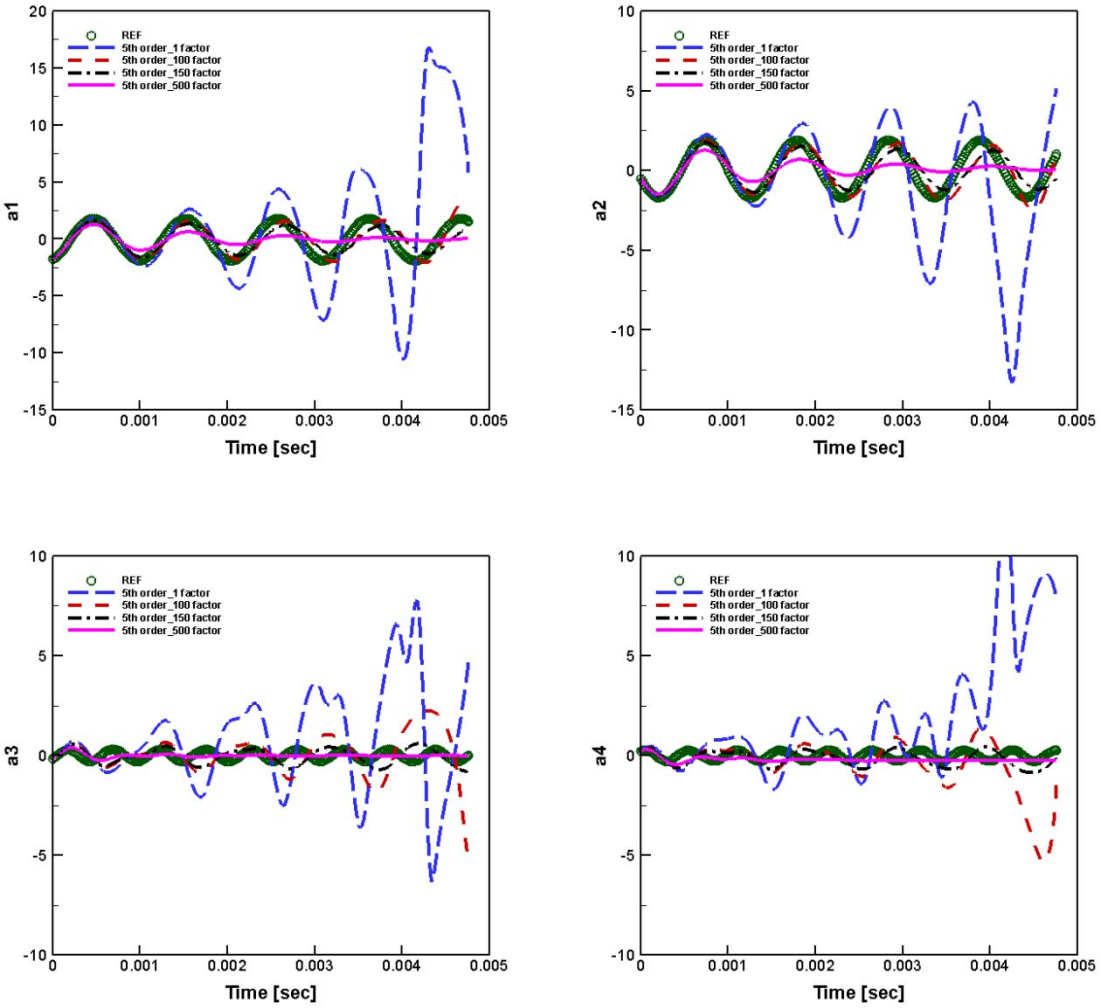

Figure 23: Effect of numerical scaling factor with 5th order scheme (sample box size : 51 x 6 x 21, Time step: 2.38E-05 sec, cycle for vortex shedding:5)

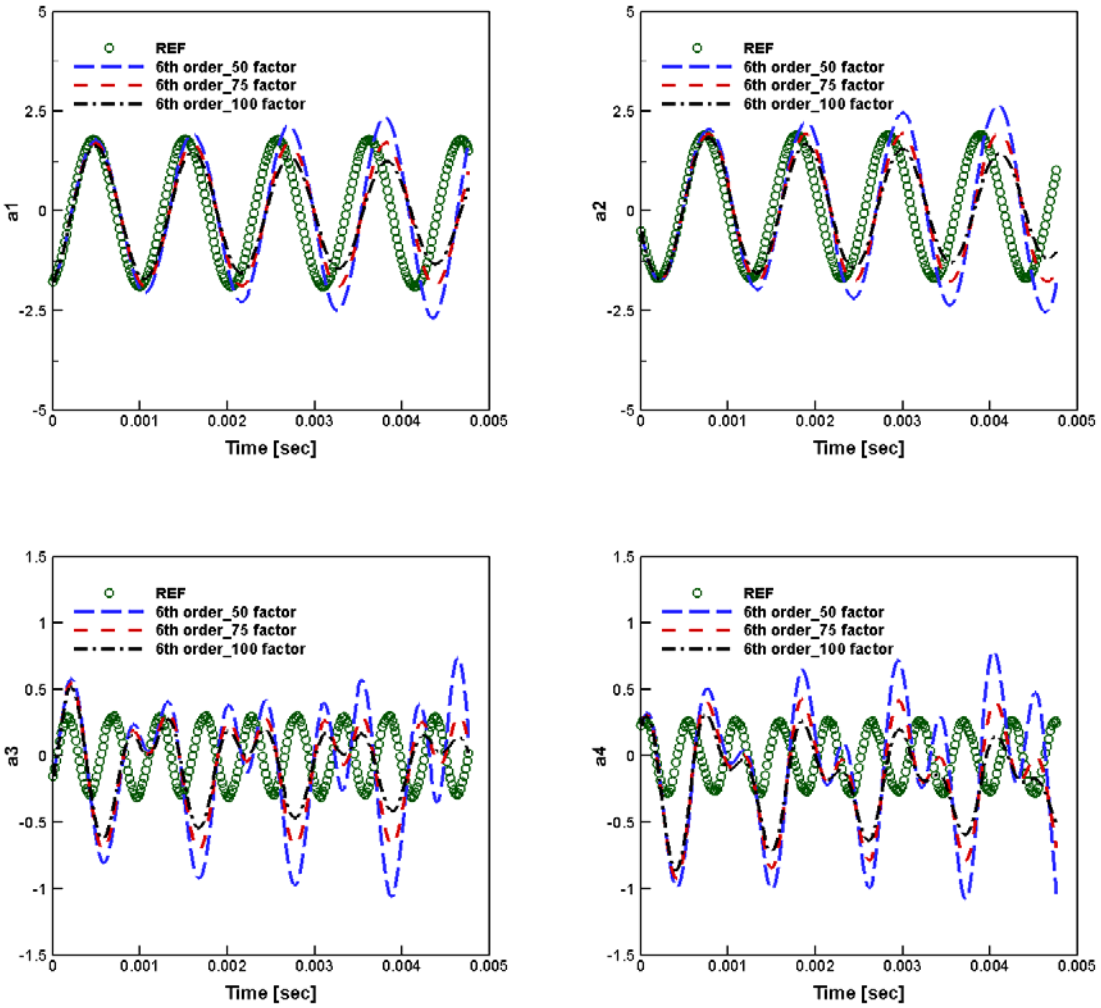

Figure 24: Effect of numerical scaling factor with 6th order scheme (sample box size : 51 x 6 x 21, Time step: 2.38E-05 sec, cycle for vortex shedding:5)

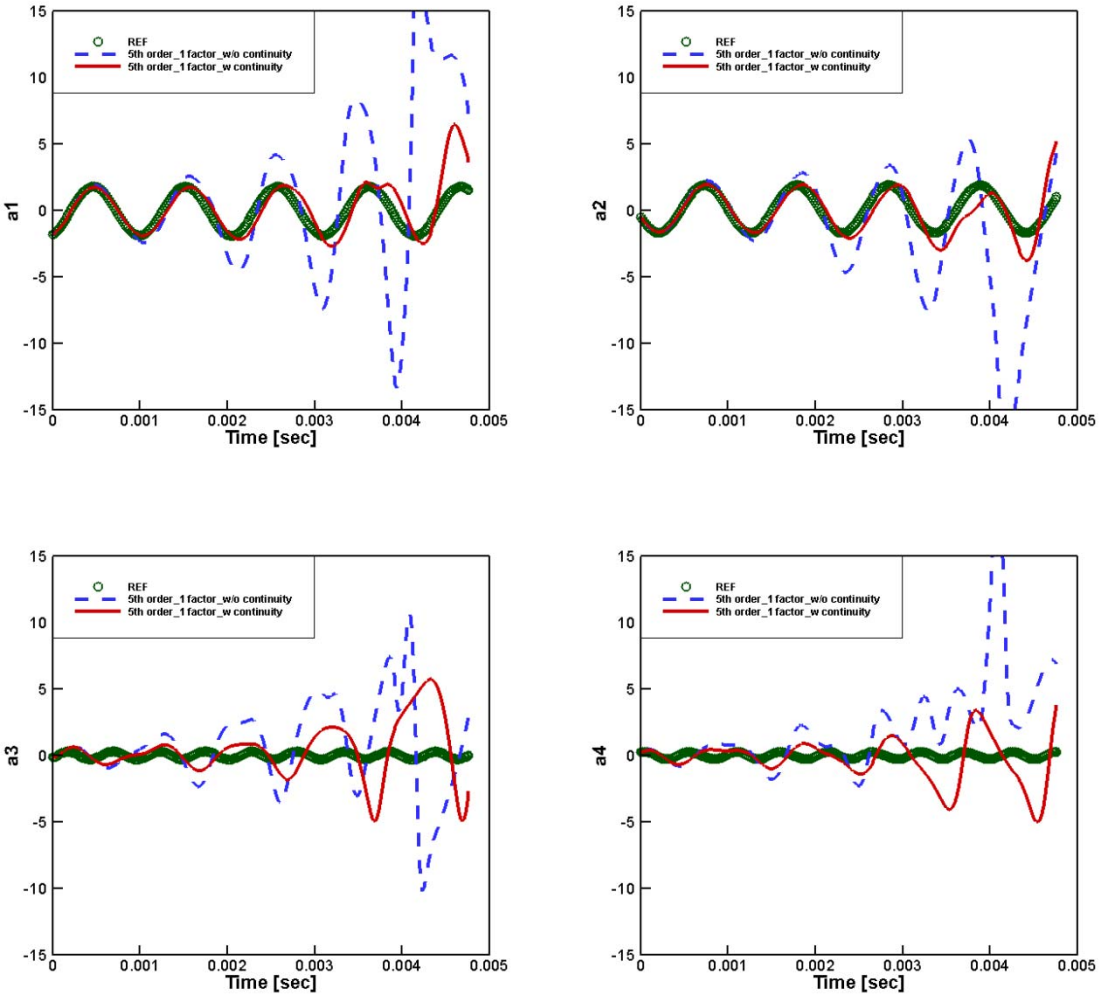

Figure 25: Effect of considering continuity term (sample box size : 51 x 6 x 21, Time step: 2.38E-05 sec, cycle for vortex shedding:5)

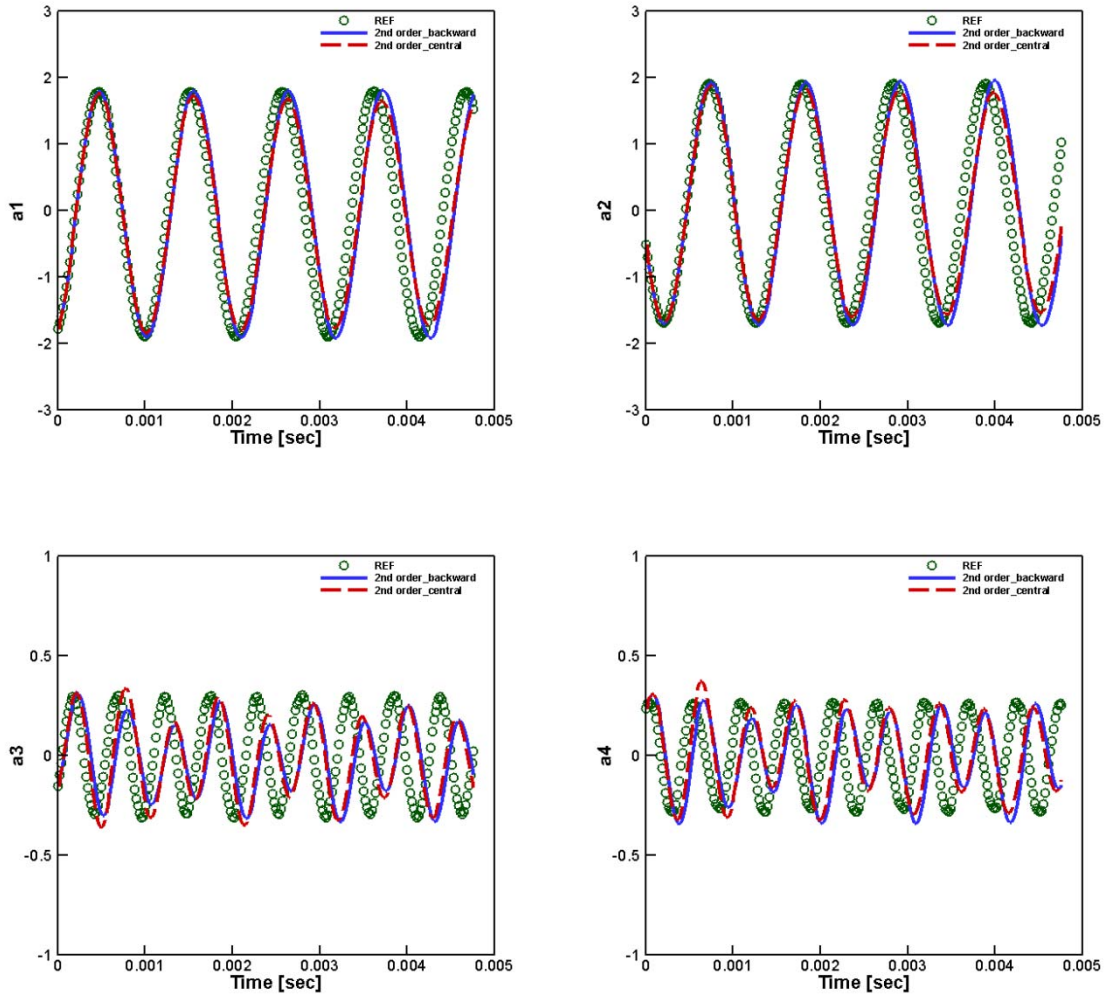

Figure 26: Comparison between backward and central scheme fixed scaling factor 1300 (sample box size : 51 x 6 x 21, Time step: 2.38E-05 sec, cycle for vortex shedding:5)

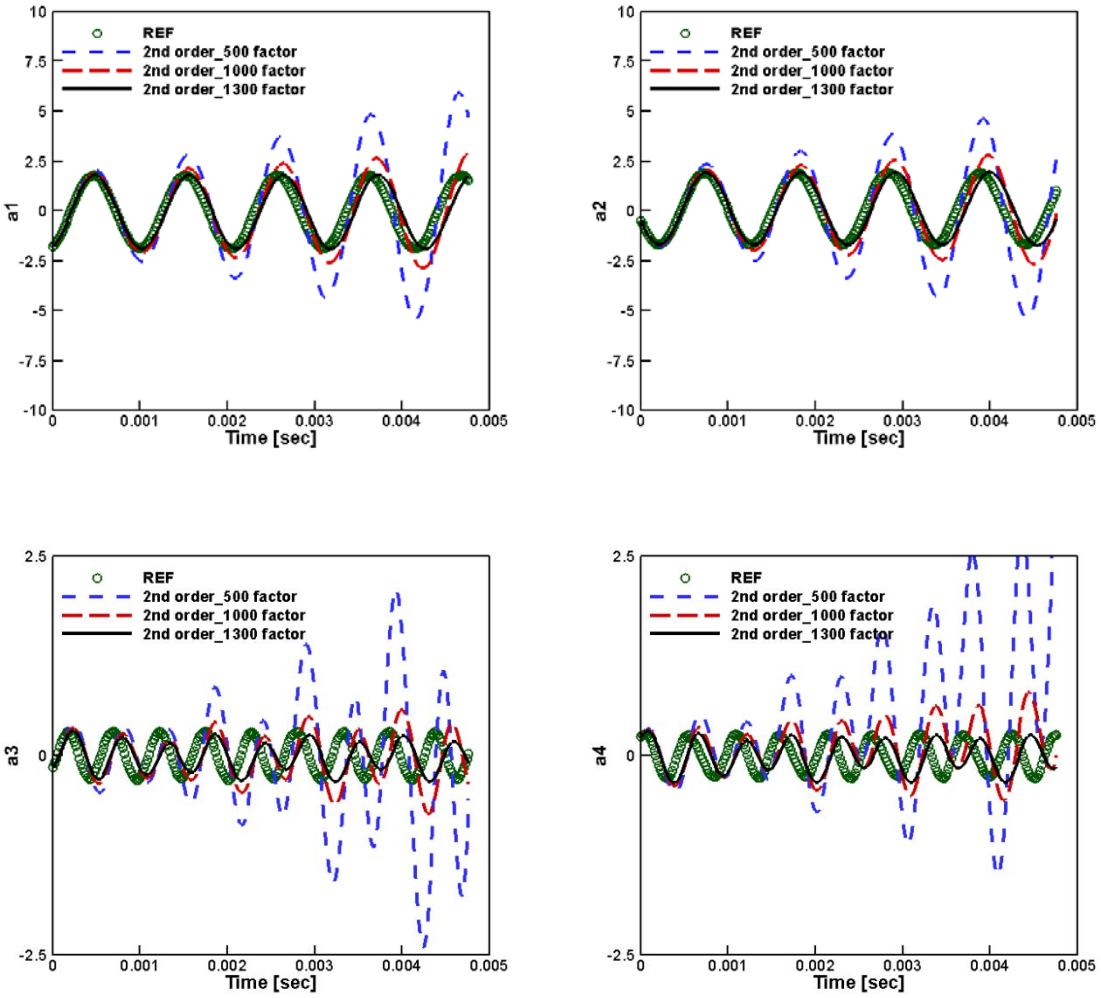

Figure 27: Effect of scaling factor with 2nd order scheme (sample box size : 51 x 6 x 21, Time step: 2.38E-05 sec, cycle for vortex shedding:5)

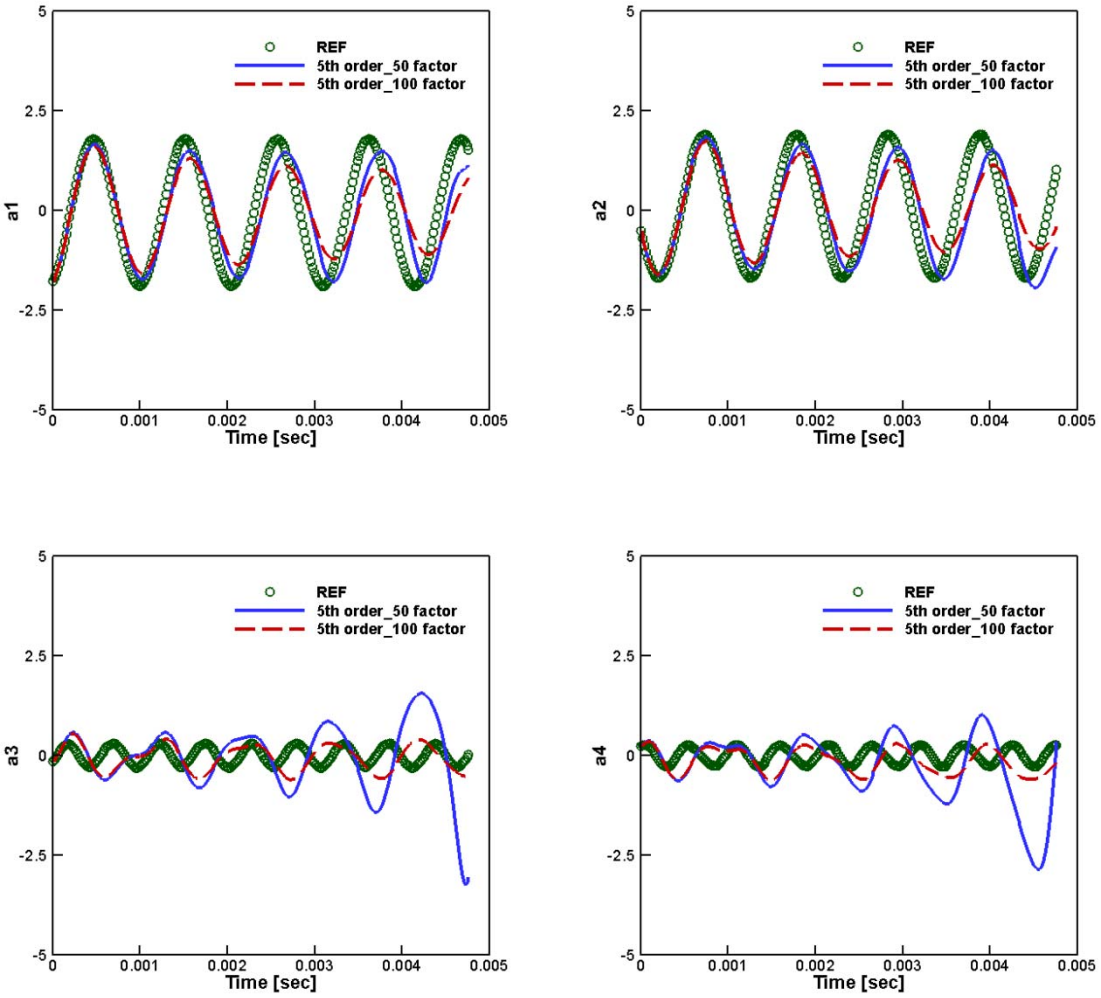

Figure 28: Effect of scaling factor with 5th order scheme (sample box size : 51 x 6 x 21, Time step: 2.38E-05 sec, cycle for vortex shedding:5)

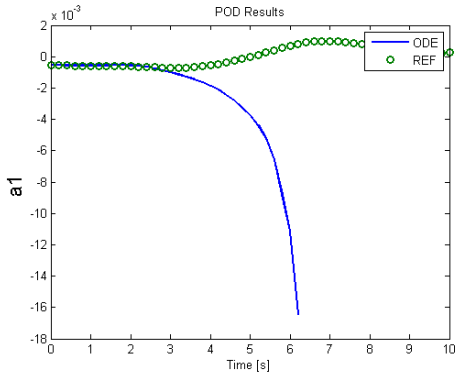

(a) Temporal evolutions of the predicted POD coefficients

Mode	Eigenvalue
1	1.1313 +12.4195i
2	1.1313 -12.4195i
3	1.0946 + 9.5968i
4	1.0946 - 9.5968i
5	0.8147 + 8.0008i
6	0.8147 - 8.0008i
7	0.4078
8	0.9604 + 2.4822i
9	0.9604 - 2.4822i
10	1.6444 + 3.8344i
11	1.6444 - 3.8344i
12	1.1713 + 5.8961i
13	1.1713 - 5.8961i

(b) Stability check : eigenvalues of linear term

Figure 29: ROM results of SFS2 case without scaling factor (sample box size : 80 x 40 x 25, Time step: 0.1 sec, theshold: 0.99)

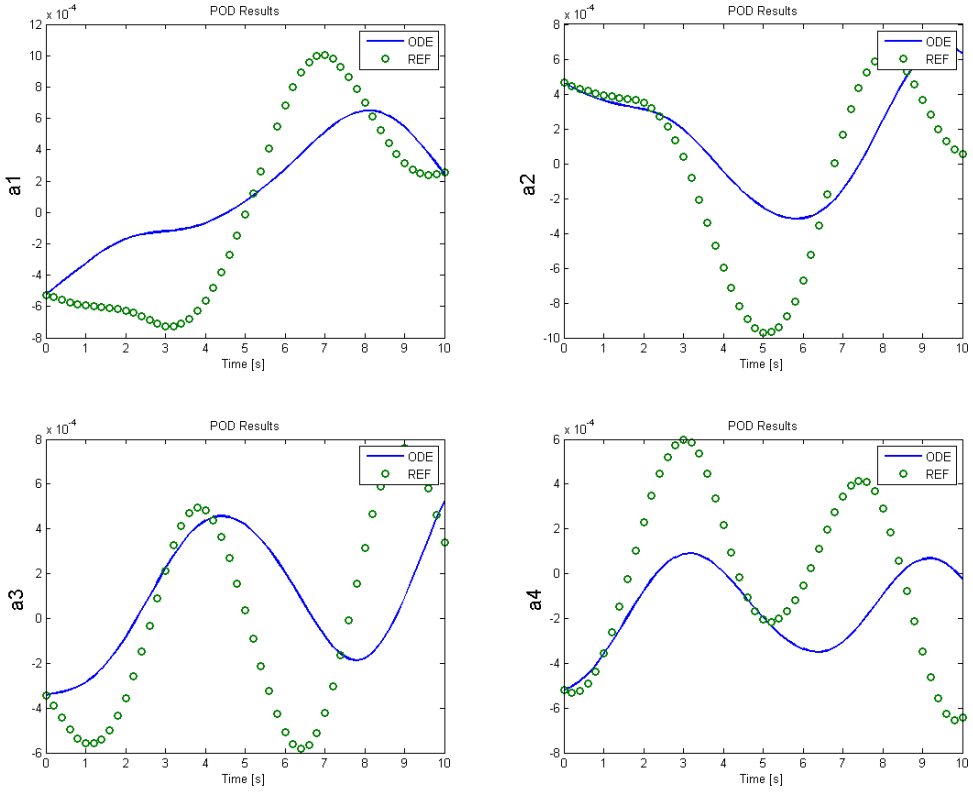

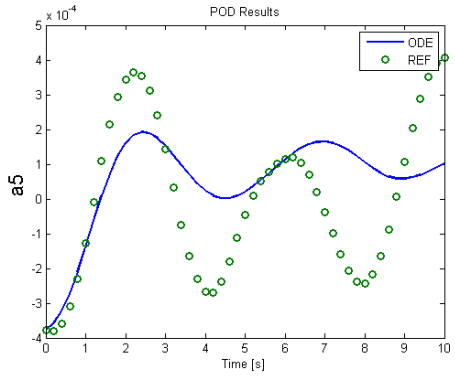
POD Results
ODE
REF
a5
Time [s]

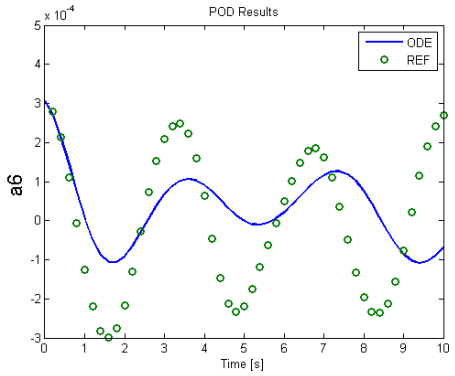
POD Results
ODE
REF
a6
Time [s]

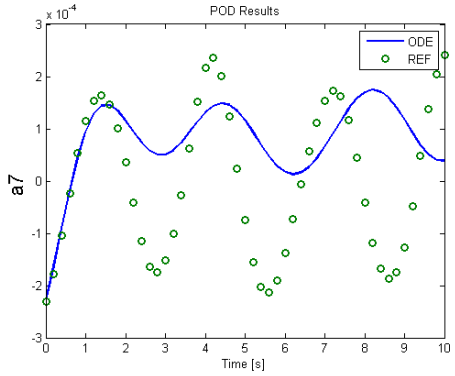
POD Results
ODE
REF
a7
Time [s]

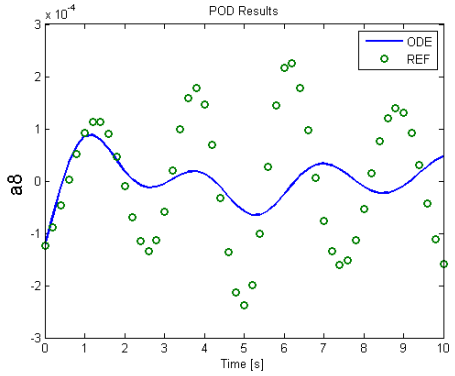
POD Results
ODE
REF
a8
Time [s]

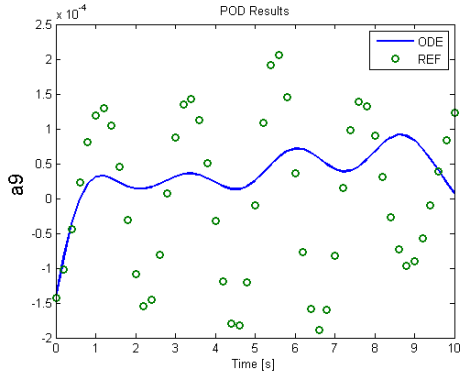
POD Results
ODE
REF
a9
Time [s]

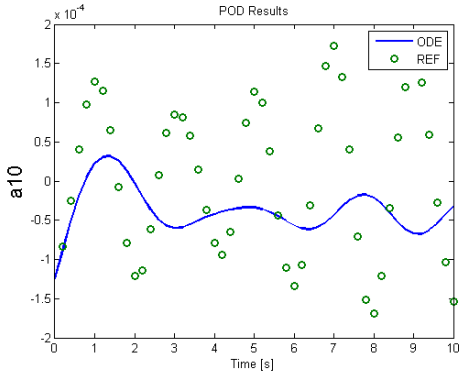
POD Results
ODE
REF
a10
Time [s]

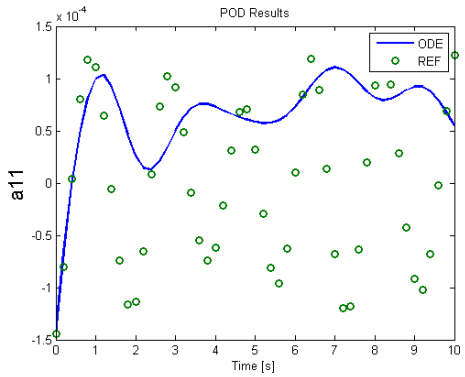
POD Results
ODE
REF
a11
Time [s]

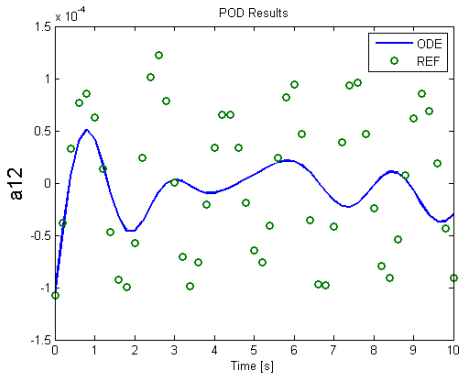
POD Results
ODE
REF
a12
Time [s]

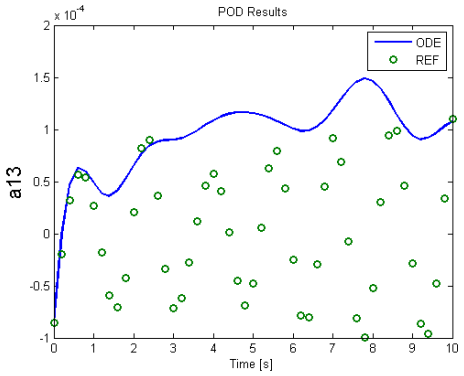

(a) Temporal evolutions of the predicted POD coefficients

Mode	Eigenvalue
1	-3.0520 +12.2633i
2	-3.0520 -12.2633i
3	-3.0351 + 9.2775i
4	-3.0351 - 9.2775i
5	-2.2757 + 8.4401i
6	-2.2757 - 8.4401i
7	-2.2203
8	-0.7533 + 2.5894i
9	-0.7533 - 2.5894i
10	0.2292 + 3.6805i
11	0.2292 - 3.6805i
12	-1.5466 + 5.8823i
13	-1.5466 - 5.8823i

(b) Stability check : eigenvalues of linear term

Figure 30: ROM results of SFS2 case with 2nd order central spatial discretization scheme (sample box size : 80 x 40 x 25, Time step: 0.1 sec, theshold: 0.99, scaling factor:8000)

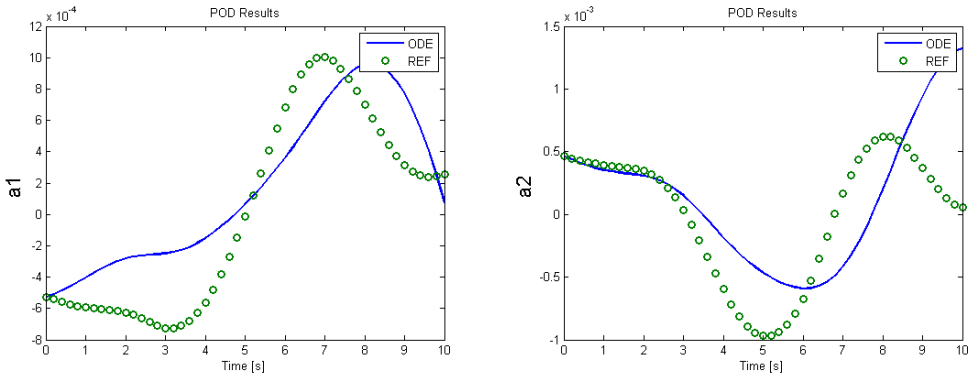

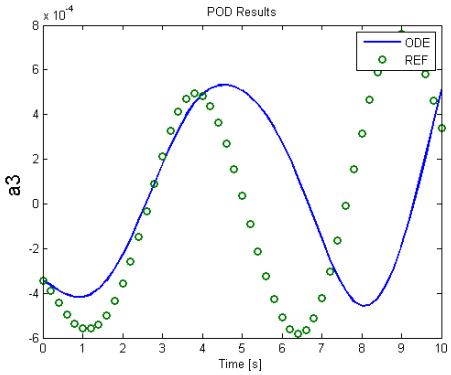
POD Results
ODE
REF
a3
Time [s]

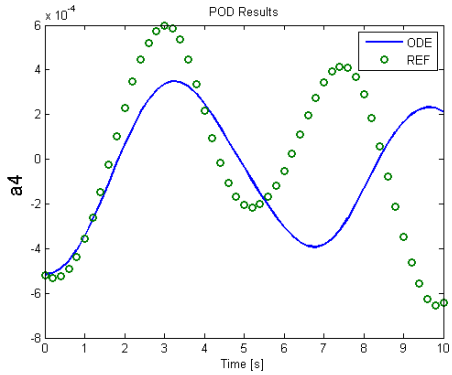
POD Results
ODE
REF
a4
Time [s]

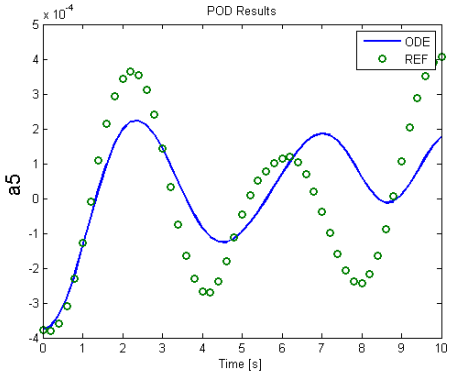
POD Results
ODE
REF
a5
Time [s]

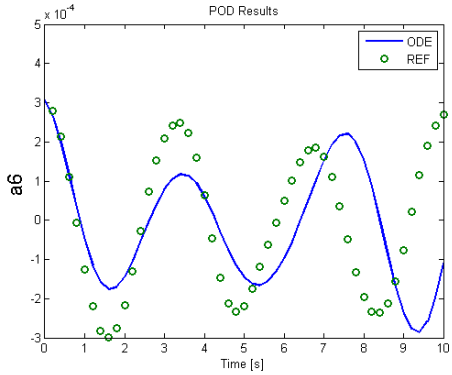
POD Results
ODE
REF
a6
Time [s]

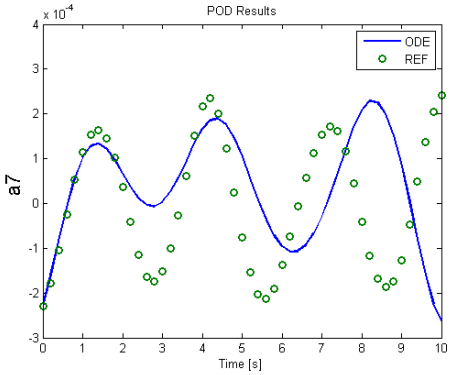
POD Results
ODE
REF
a7
Time [s]

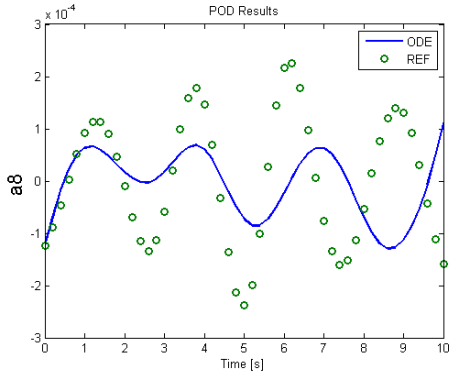
POD Results
ODE
REF
a8
Time [s]

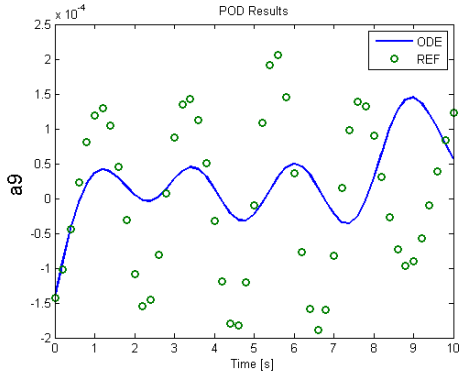
POD Results
ODE
REF
a9
Time [s]

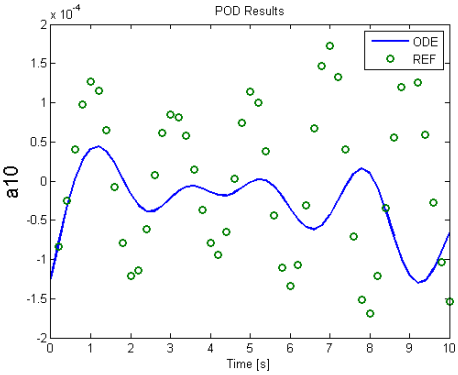
POD Results
ODE
REF
a10
Time [s]

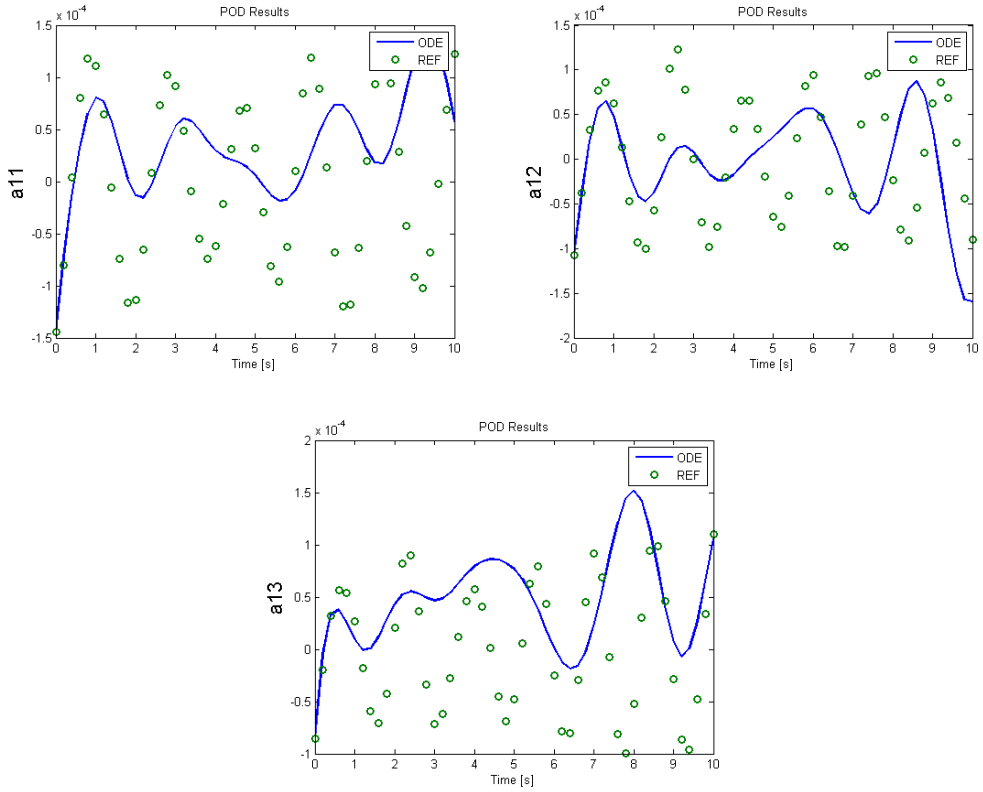

(a) Temporal evolutions of the predicted POD coefficients

Mode	Eigenvalue
1	-3.3227 +12.9183i
2	-3.3227 -12.9183i
3	-2.9679 + 9.9939i
4	-2.9679 - 9.9939i
5	-2.3976 + 8.3495i
6	-2.3976 - 8.3495i
7	-1.7370
8	-0.4896 + 2.6983i
9	-0.4896 - 2.6983i
10	0.2294 + 3.7406i
11	0.2294 - 3.7406i
12	-1.5696 + 6.0945i
13	-1.5696 - 6.0945i

(b) Stability check : eigenvalues of linear term

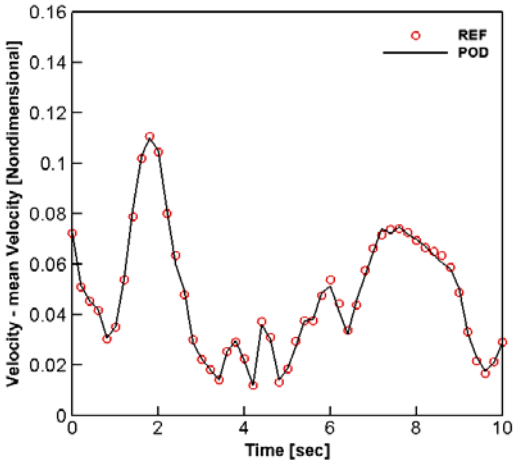

(c) Comparison of velocity between CFD and POD analysis

Figure 31: ROM results of SFS2 case with 5th order backward spatial discretization scheme (sample box size : 80 x 40 x 25, Time step: 0.1 sec, theshold: 0.99, scaling factor:800)

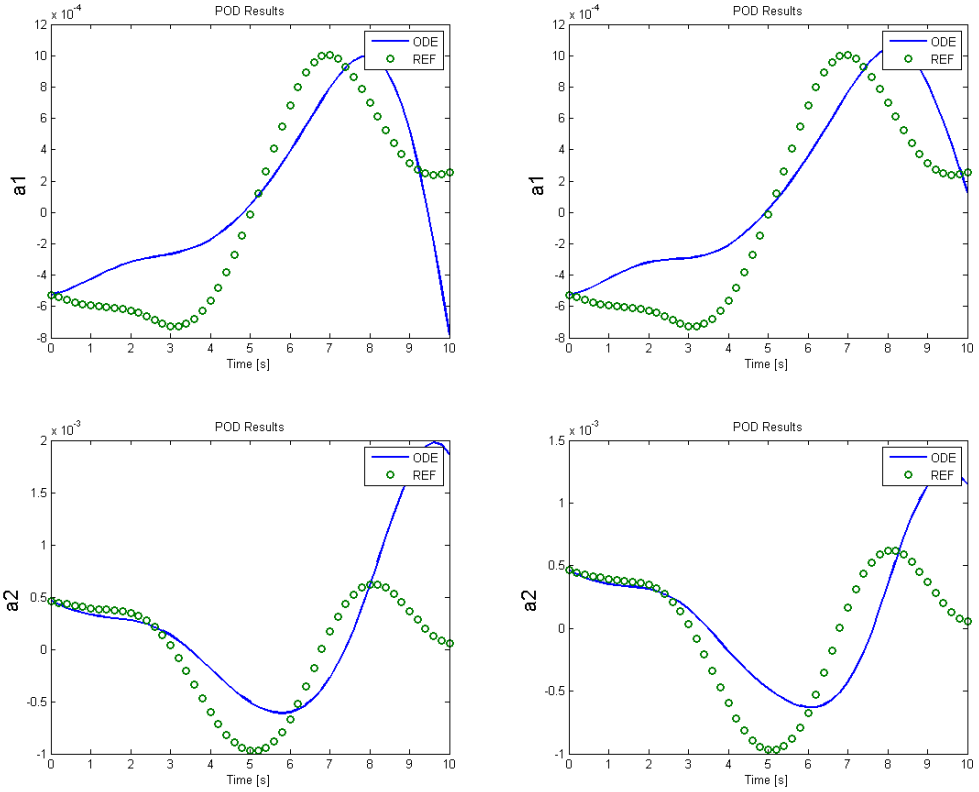

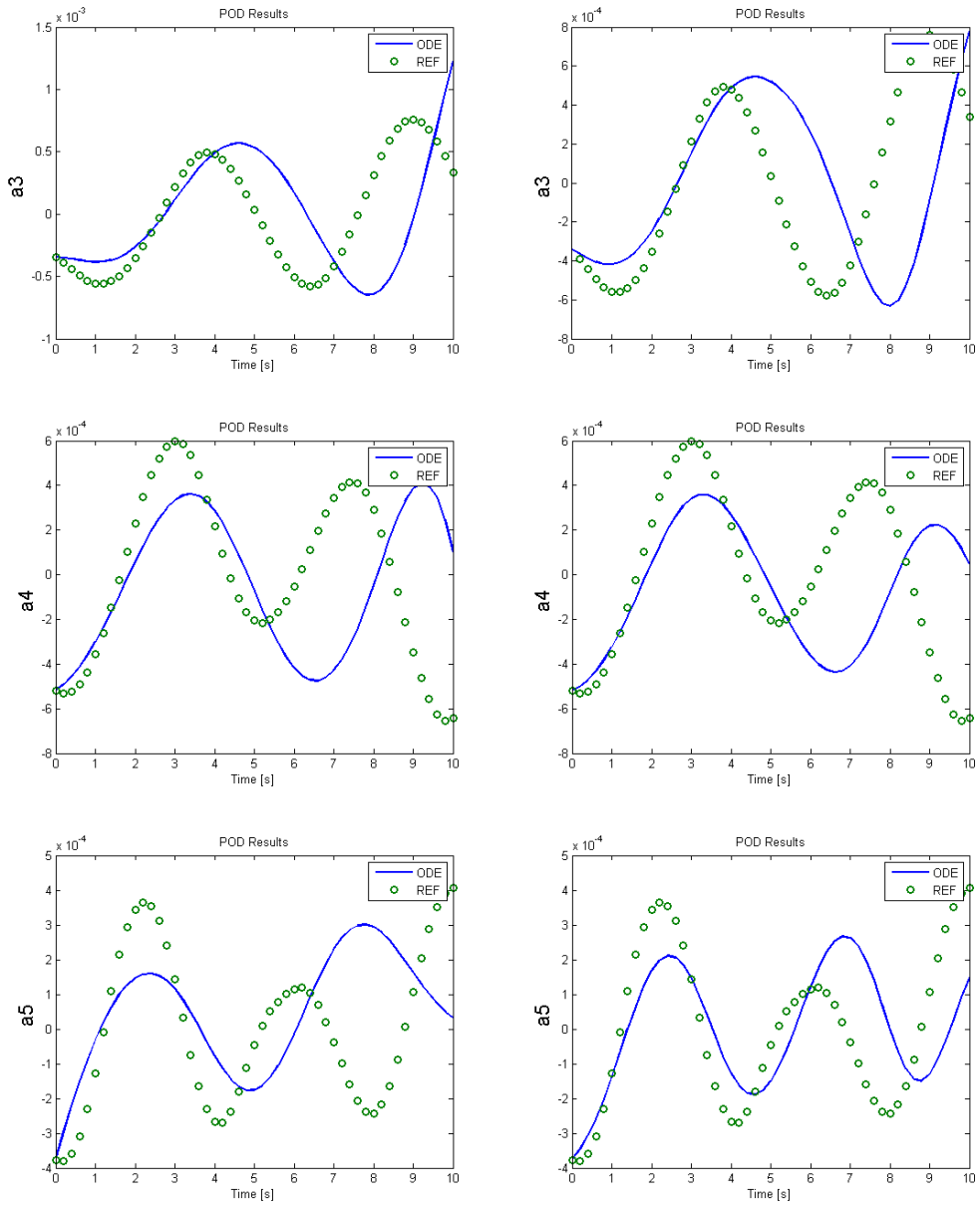

(a) Temporal evolutions of the predicted POD coefficients, Left : 90%, Right : 95%

Figure 32: Effect of threshold (sample box size: 80 x 40 x 25, Time step: 0.1 sec, scaling factor: 800, 5th order backward spatial discretization scheme)

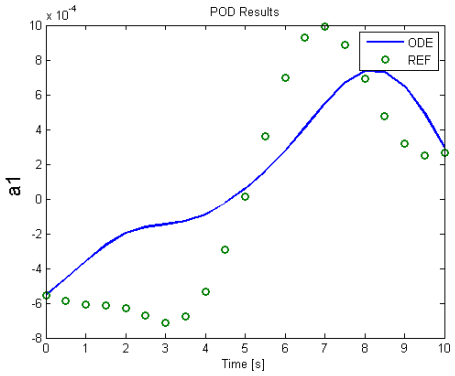
POD Results
x 10^-4
ODE
REF
a1
Time [s]

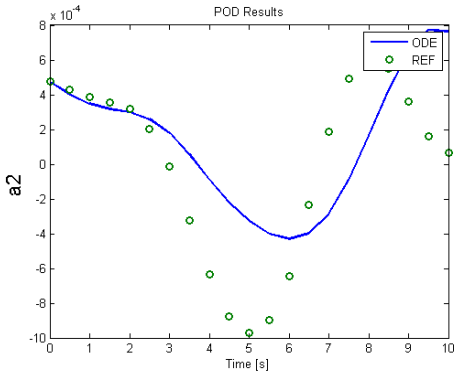
POD Results
x 10^-4
ODE
REF
a2
Time [s]

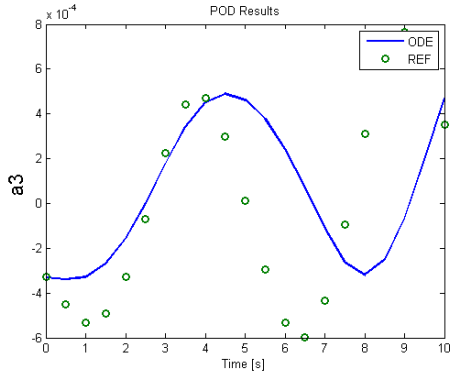
POD Results
x 10^-4
ODE
REF
a3
Time [s]

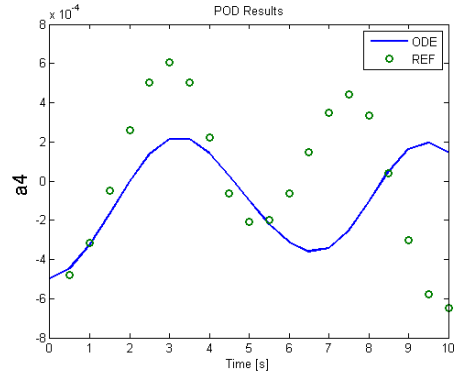
POD Results
x 10^-4
ODE
REF
a4
Time [s]

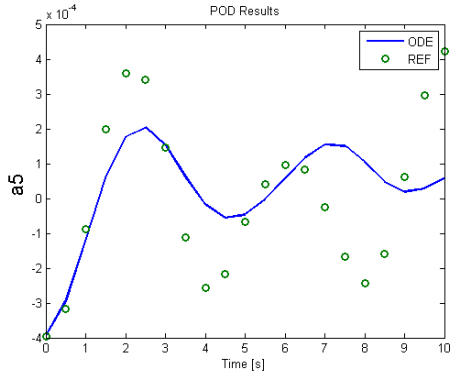
POD Results
x 10^-4
ODE
REF
a5
Time [s]

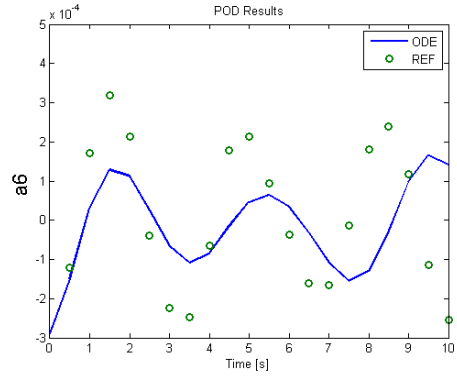
POD Results
x 10^-4
ODE
REF
a6
Time [s]

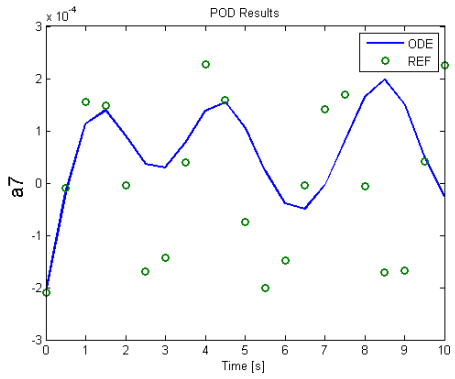
POD Results
x 10^-4
ODE
REF
a7
Time [s]

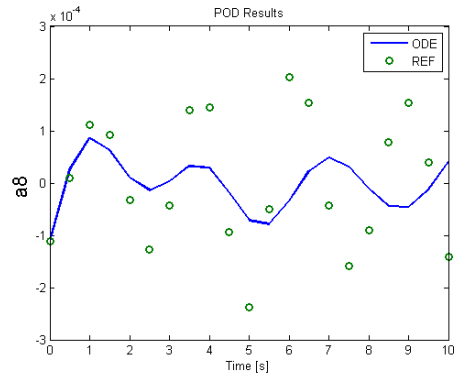
POD Results
x 10^-4
ODE
REF
a8
Time [s]

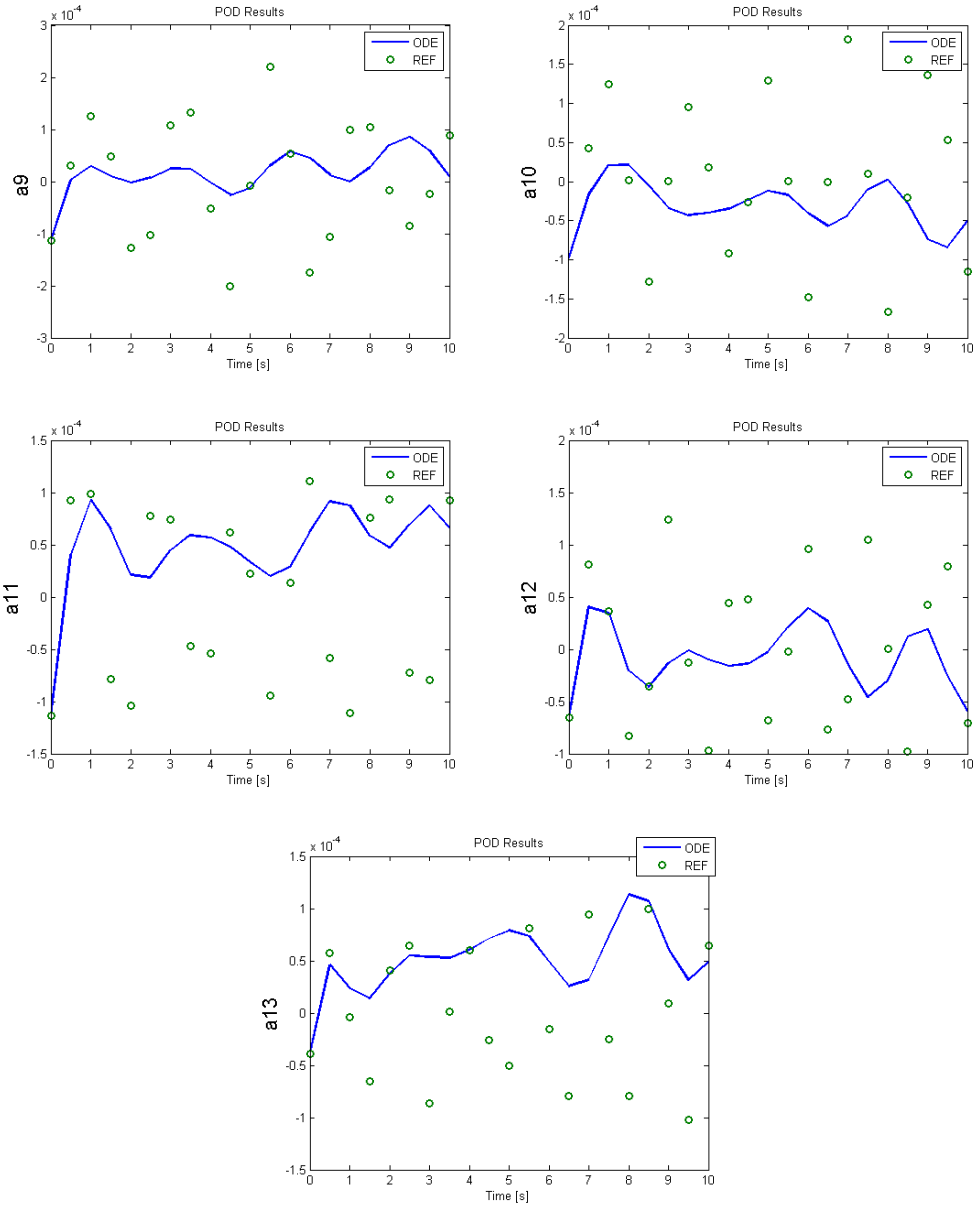

(a) Temporal evolutions of the predicted POD coefficients

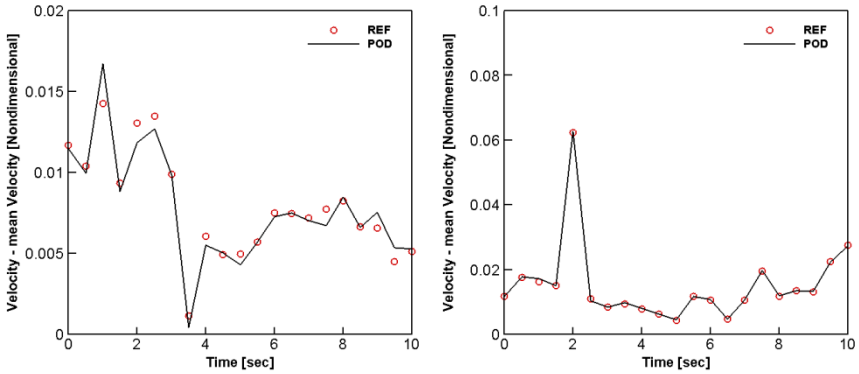

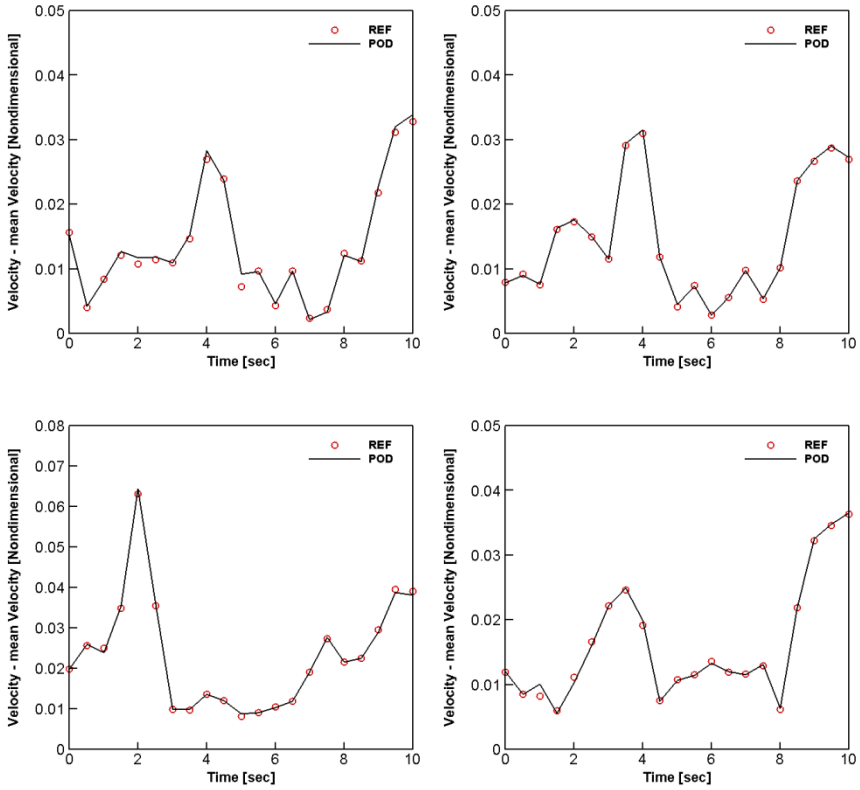

(b) Comparison of velocity between CFD and POD analysis

Figure 33: ROM results of SFS2 case with 2nd order backward spatial discretization scheme (sample box size: 120 x 65 x 30, Time step: 0.5 sec, theshold: 0.99, scaling factor: 7500)

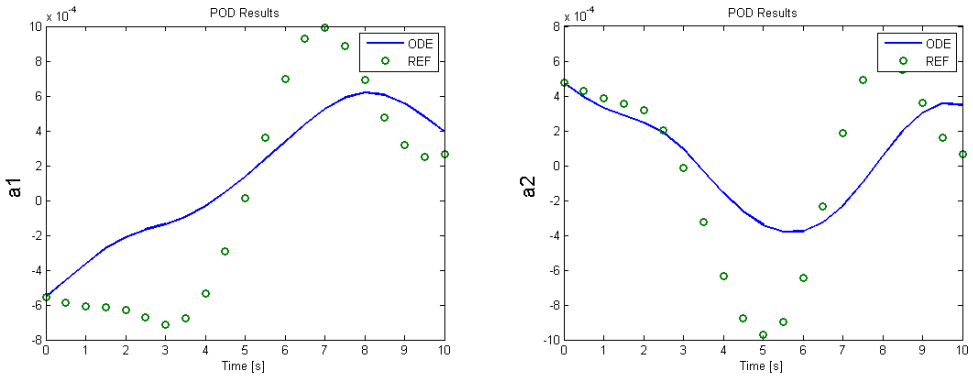

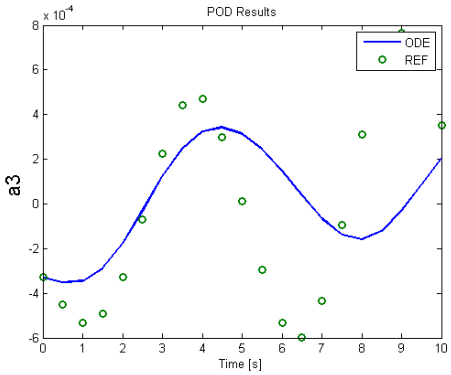
POD Results
ODE
REF
a3
Time [s]

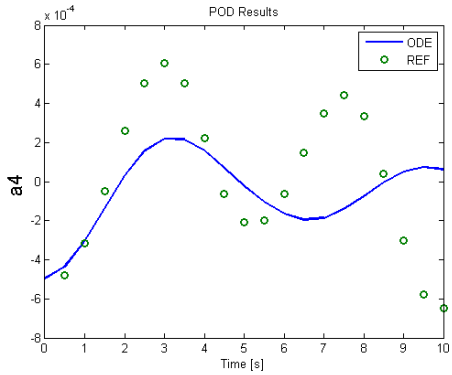
POD Results
ODE
REF
a4
Time [s]

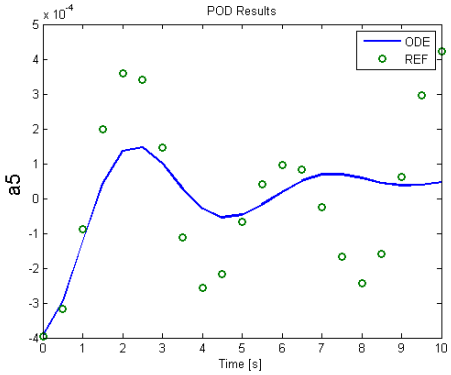
POD Results
ODE
REF
a5
Time [s]

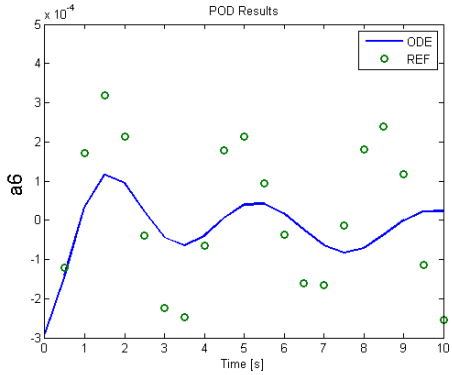
POD Results
ODE
REF
a6
Time [s]

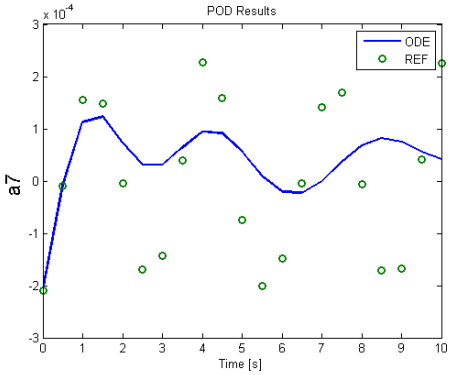
POD Results
ODE
REF
a7
Time [s]

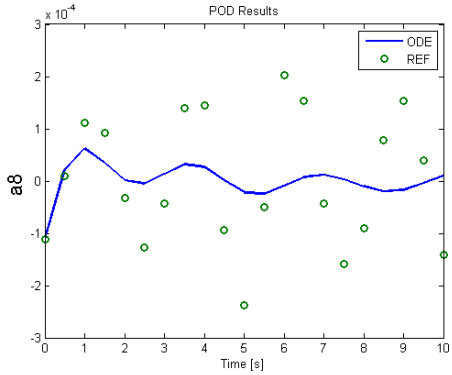
POD Results
ODE
REF
a8
Time [s]

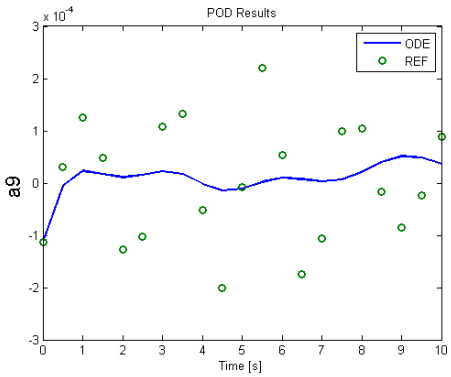
POD Results
ODE
REF
a9
Time [s]

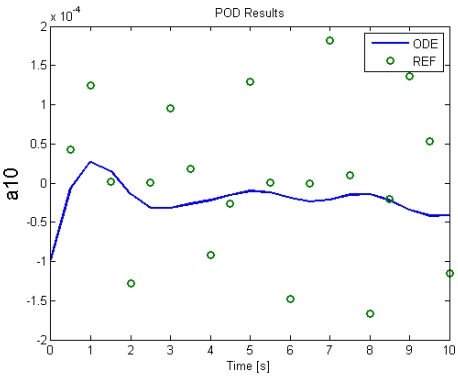
POD Results
ODE
REF
a10
Time [s]

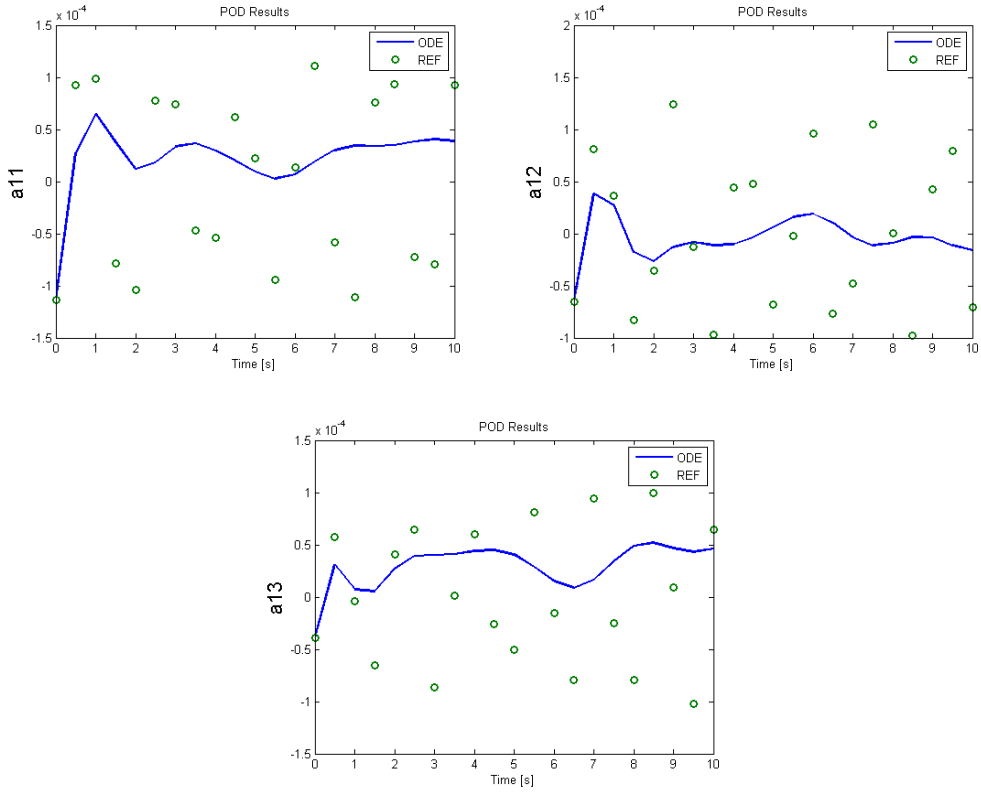

Figure 34: ROM results of SFS2 case with 5th order backward spatial discretization scheme (sample box size: 120 x 65 x 30, Time step: 0.5 sec, theshold: 0.99, scaling factor: 800)